Inorganic Chemistry

Article

pubs.acs.org/IC

Lead(II) Complex Formation with Glutathione

Vicky Mah and Farideh Jalilehvand*

Department of Chemistry, University of Calgary, 2500 University Drive NW, Calgary, Alberta T2N 1N4, Canada

Supporting Information

ABSTRACT: A structural investigation of complexes formed between the Pb^{2+} ion and glutathione (GSH, denoted AH_3 in its triprotonated form), the most abundant nonprotein thiol in biological systems, was carried out for a series of aqueous solutions at pH 8.5 and $C_{Pb^{2+}}$ = 10 mM and in the solid state. The Pb L_{III}-edge extended X-ray absorption fine structure (EXAFS) oscillation for a solid compound with the empirical formula $[Pb(AH_2)]ClO_4$ was modeled with one Pb−S and two short Pb−O bond distances at 2.64 ± 0.04 and 2.28 ± 0.04 Å, respectively. In addition, Pb···Pb interactions at 4.15 ± 0.05 Å indicate dimeric species in a network where the thiolate group forms an asymmetrical bridge between two Pb^{2+} ions. In aqueous solution at the mole ratio GSH/Pb^{II} = 2.0 ($C_{Pb^{2+}}$ = 10 mM, pH 8.5), lead(II) complexes with two thiolate ligands form, characterized by a ligand-to-metal charge-transfer band (LMCT) $S^- \rightarrow Pb^{2+}$ at 317 nm in the UV−vis spectrum and mean Pb−S and Pb−(N/O) bond distances of 2.65 ± 0.04 and 2.51 ± 0.04 Å, respectively, from a Pb L_{III}-edge EXAFS spectrum. For solutions with higher mole ratios, $GSH/Pb^{II} \geq 3.0$, electrospray ionization mass spectroscopy spectra identified a triglutathionyllead(II) complex, for which Pb L_{III}-edge EXAFS spectroscopy shows a mean Pb−S distance of 2.65 ± 0.04 Å in PbS_3 coordination, ^{207}Pb NMR spectroscopy displays a chemical shift of 2793 ppm, and in the UV−vis spectrum, an $S^- \rightarrow Pb^{2+}$ LMCT band appears at 335 nm. The complex persists at high excess of GSH and also at ∼25 K in frozen glycerol (33%)/water glasses for GSH/Pb^{II} mole ratios from 4.0 to 10 ($C_{Pb^{2+}}$ = 10 mM) measured by Pb L_{III}-edge EXAFS spectroscopy.

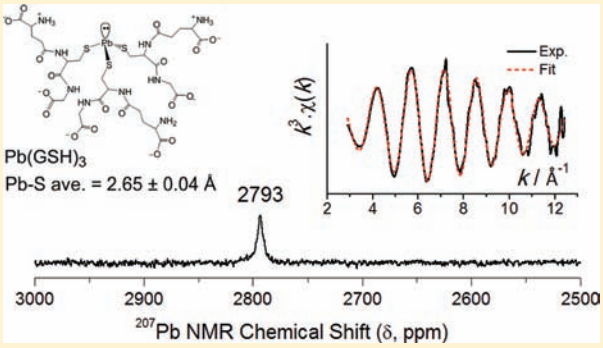

INTRODUCTION

The toxicology of divalent lead is complex and is known to adversely affect the function of organ systems in the human body including the kidneys and developing blood cells, as well as the central nervous and reproductive systems.[1−3] The toxic effects are frequently attributed to the displacement of essential metals (e.g., Ca^{2+} and Zn^{2+}) by the Pb^{2+} ion, which along with simultaneous binding to structural and catalytic protein sites disturbs normal biological activity.[4−6] One of the major targets identified for the Pb^{2+} ion is δ-aminolaevulinic acid dehydratase (ALAD), a key zinc-containing metalloenzyme in the heme biosynthetic pathway for forming important tetrapyrroles such as heme, corrin, and chlorophyll.[6] In human erythrocytes, Pb^{2+} ions bind to ALAD with 25-fold higher affinity than Zn^{2+} ions.[7] Consequently, patients suffering from lead poisoning are often afflicted with anemia.[8] The native ALAD enzyme has tetrahedral coordination geometry around the Zn^{2+} ion in its active site, while X-ray crystallography of Pb^{2+}-substituted ALAD in yeast reveals that the Pb^{2+} ion coordinates to the thiol groups of three cysteinyl residues in trigonal-pyramidal geometry,[9] which may, in part, explain inhibition of the ALAD enzymatic activity in the presence of Pb^{2+} ions.[10−12] Spectroscopic studies show that the Pb^{2+} ion also tends to coordinate three thiolate ligands when occupying the domains in sulfur-rich proteins that normally contain Zn^{2+} ions, as well as when bound to the metalloregulatory proteins CadC and AztR found in prokaryotes.[13−18] In comparison, little information is available on the structure of lead(II) complexes with thiolate ligands in small molecules,[19] which are commonly found within cells or exogenously administered as heavy-metal chelating agents.

The Pb^{2+} ion displays a large range of coordination numbers often in an irregular coordination geometry.[20,21] At low coordination numbers, a void often appears in a distorted (*hemidirected*) structure, a phenomenon that traditionally has been ascribed to an inert, sterically active lone pair of electrons, originating from 6s6p orbital mixing for the Pb^{2+} ion. However, density functional theory calculations have in recent years modified this picture and show that asymmetries in the valence-shell electron densities that result from direct electronic interactions between the cation and its ligands are the cause of the distorted structures in lead(II) complexes.[22−24] The covalent interaction between filled ligand orbitals (e.g., O 2p) and the Pb^{2+} $6s^2$ and empty 6p orbitals can create bonding and antibonding molecular orbitals (MOs).[22] A lone pair in such an antibonding MO creates a void by repelling the ligands, which increases the ligand−ligand repulsion and counteracts an increase in the coordination number. The combination of those counteracting effects will establish whether a regular (*holodirected*) or a distorted (*hemidirected*) structure corresponds to an energy minimum. The regular structure for the

Received: March 6, 2012
Published: May 17, 2012

   dx.doi.org/10.1021/ic300496t | Inorg. Chem. 2012, 51, 6285−6298

solid PbS compound with the Pb^{2+} ion surrounded by six sulfide ions (as in NaCl), in contrast to the distorted structure of PbO with four asymmetrically distributed oxide ions, has been attributed to a weaker electronic interaction because of the greater mismatch between the Pb^{2+} 6s and S 3p atomic orbitals than with O 2p.[22] For high coordination numbers or space-demanding ligands, the increase in the ligand−ligand repulsion strongly promotes regular (*holodirected*) structures.[21]

Glutathione (γ-L-glutamyl-L-cysteinylglycine, GSH, denoted AH_3 in its triprotonated form; Scheme 1) is a ubiquitous

Scheme 1. Dominant Form (AH^{2-}) of GSH at pH ∼9[38]

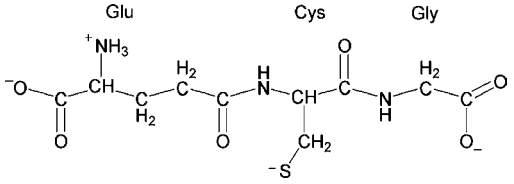

tripeptide found in the cells of plants, animals, and microorganisms at relatively high concentrations (0.1−10 mM).[25,26] Among its many vital roles, GSH protects cellular membranes from the toxic effects of heavy metals (e.g., Pb^{2+}, Hg^{2+}, Cd^{2+}) by complex formation, before they are transferred to higher-molecular-weight cysteine-rich peptides such as metallothioneins and phytochelatins, which remove the harmful metal ions.[27−33] Toxicological studies have shown that patients exposed to lead occupationally obtain decreased levels of GSH in their blood, suggesting that Pb^{2+}-GSH complexes are formed in vivo.[34−36] Gold nanoparticles with GSH as the functional group were recently introduced as a highly selective/sensitive colorimetric probe for detecting Pb^{2+} ions in aqueous environmental/biological samples.[37]

The microscopic acid dissociation constants for GSH have been directly determined using ^{1}H NMR spectroscopy, showing that the two carboxylic acid groups deprotonate simultaneously over the pH range 0.5−6 (pK_{a1} = 2.19 for glutamyl and pK_{a2} = 3.22 for glycyl), while the cysteinyl thiol group loses its proton concurrently to the ammonium group (pK_{a3} = 8.97 and pK_{a4} = 9.17, respectively) over the pH range 7−12.[39]

The complex formation between GSH and Pb^{2+} ions in aqueous solution has previously been studied by ^{13}C and ^{1}H NMR methods within the pD range 5.4−12.[40,41] The ^{1}H NMR studies suggest that the Pb^{2+} ion binds exclusively to the cysteinyl S-donor atom of GSH.[41] However, for a Pb^{2+}-GSH solution with a mole ratio GSH/Pb^{2+} = 2.0 at pD < 9, the ^{13}C NMR results indicate minor interactions also between Pb^{2+} and the glycine carboxylate group. Under acidic conditions (pD 2.3−5.4), the appearance of white precipitates restricted solution studies by NMR spectroscopy.[40] Solid precipitates with the general formula $[Pb(AH_2)X]\cdot H_2O$ (where X = Cl, NO_3^-, CH_3COO^-, or NCS^-) were identified with the cysteinyl thiolate coordinated to the Pb^{2+} ion, as evidenced by the absence of the ν(S−H) band in the IR spectra.[42]

An earlier potentiometric study of a dilute Pb^{2+} solution containing $C_{Pb^{2+}}$ = 5 mM and C_{GSH} = 10 mM resulted in a [Pb(AH)] complex as the major species formed at pH ∼5,[43] while $[Pb(A)]^-$ and $[Pb(GSH)_2]^{n-}$ (n = 2−4) complexes predominate at higher pH values (between 7.0 and 10.0).[43] The m/z peaks in electrospray ionization mass spectroscopy (ESI-MS) spectra for $[Pb(AH_2)]^+$ and $[Pb(A)]^-$ species were detected in both the positive and negative modes for a solution containing equimolar amounts (0.033 M) of Pb^{2+} and GSH,[44] while both mononuclear $[Pb(AH)_2]^{2-}$ and dinuclear $[Pb_2(AH)_2]$ complexes were proposed to form between pH 5.5 and 7.0 in a polarographic study.[45]

Further insight into the nature and structure of the complexes formed between Pb^{2+} ions and GSH in solution, including the number of donor atoms, their bond distances, and the coordination geometry about the metal center, is clearly needed. In a continuation of our systematic structural studies of complexes formed between toxic metal ions and biologically relevant small molecular ligands,[46−51] the present structural study of Pb^{2+}-GSH complexes was carried out using a combination of spectroscopic techniques, i.e., Pb L_{III}-edge X-ray absorption spectroscopy (XAS), ^{207}Pb and ^{1}H NMR, ESI-MS, and UV−vis. To promote the formation of higher complexes, pH 8.5 was chosen to increase the amount of deprotonated thiolate groups in aqueous solution. The preliminary ^{207}Pb NMR chemical shifts reported in Mah's Ph.D. thesis,[52] for the Pb^{2+} ion bound to this biologically important thiol-containing ligand, showed that ^{207}Pb NMR spectroscopy is a very useful tool for structural characterizations of Pb^{2+}-substituted proteins. This is evidenced in recent reports where ^{207}Pb NMR spectroscopy was used (1) to investigate the lead(II) environment in thiol-rich proteins,[53,54] (2) to propose that a $[Pb(GS)_3]^-$ complex can form with GSH in solutions with pH 7.5−9.5,[55] and (3) to reveal that two different trigonal-pyramidal PbS_3 environments can be formed in the zinc binding domain in the HIV nucleocapsid protein HIV-CCHC.[55]

Nowadays, extended X-ray absorption fine structure (EXAFS) spectra are often measured at low temperature (LT) to avoid photoreduction of the absorbing atom and to extend the useful k range of the data by reducing thermal disorder.[56] Recently, we showed for a series of Hg^{2+}-GSH and Cd^{2+}-GSH alkaline solutions that the EXAFS structural parameters obtained from such LT measurements can differ from room-temperature (RT) results, corresponding to an increasing stability of higher complexes at LT for strongly exothermic reactions.[50,51] In the current study, the effect of the temperature on the speciation of Pb^{2+}-GSH complexes formed in solution was evaluated by comparing Pb L_{III}-edge EXAFS spectra obtained at RT with those obtained for frozen glasses at ∼25 K with similar concentration but with 33% (v/v) glycerol added.

EXPERIMENTAL SECTION

Sample Preparation. Glutathione (GSH), sodium hydroxide, and $Pb(ClO_4)_2\cdot 3H_2O$ were purchased from Sigma-Aldrich and used without further purification. Syntheses were carried out under an inert argon atmosphere, and the pH of the aqueous solutions was monitored with a Corning Semi-Micro electrode calibrated to standard buffers. All solutions were prepared using deoxygenated water, prepared by boiling distilled water and bubbling argon through to remove dissolved O_2.

To a GSH solution (1 mmol) in O_2-free H_2O (pH 2.7) was added $Pb(ClO_4)_2\cdot 3H_2O$ (0.5 mmol; pH 2.2). Upon the dropwise addition of NaOH (2 M), a white precipitate formed, which was collected at pH 2.5. The precipitate was washed with water and ether and then dried under vacuum. Elem anal. Calcd for $[Pb(AH_2)]ClO_4$ ($PbC_{10}H_{17}N_3O_{11}SCl$): C, 19.59; H, 2.63; N, 6.85. Found: C, 19.68; H, 2.73; N, 6.65.

Pb^{2+}-GSH solutions were prepared by dissolving GSH (0.1−0.5 mmol) in deoxygenated water, followed by the addition of

dx.doi.org/10.1021/ic300496t | Inorg. Chem. 2012, 51, 6285−6298

$Pb(ClO_4)_2 \cdot 3H_2O$ (0.05 mmol), thereby forming a white precipitate (pH 2.0−2.2). Sodium hydroxide (2 M) was added dropwise to the mixture until the solid dissolved at pH ∼5, giving a clear colorless solution. Five solutions with $C_{Pb^{2+}}$ = 10 mM and the GSH/Pb^{2+} mole ratios 2.0 (A), 3.0 (B), 4.0 (C), 5.0 (D), and 10.0 (E) were prepared for which the final pH was adjusted to 8.51. Solution I with higher lead(II) concentration, $C_{Pb^{2+}}$ = 90 mM, was prepared to facilitate ^{207}Pb NMR measurements at the mole ratio GSH/Pb^{2+} = 3.0 and pH 8.5

Table 1. Composition of the Pb^{2+}-GSH Solutions Studied at pH 8.5[a]

solution	GSH/Pb^{2+}	$C_{Pb^{2+}}$ (mM)	C_{GSH} (mM)
	RT Solutions		
A	2.0	10	20
B	3.0	10	30
C	4.0	10	40
D	5.0	10	50
E	10.0	10	100
I	3.0	90	270
	LT Solutions		
A*	2.0	10	20
B*	3.0	10	30
C*	4.0	10	40
D*	5.0	10	50
E*	10.0	10	100

[a]Solutions A*−E* contain 33% (v/v) glycerol added just before EXAFS measurement; the pH was measured prior to the addition of glycerol.

(Table 1). For LT (∼25 K) Pb L_{III}-edge EXAFS measurements, aqueous GSH solutions containing $C_{Pb^{2+}}$ = 15 mM were diluted with 33% (v/v) glycerol, giving a final $C_{Pb^{2+}}$ ∼ 10 mM. Prior to LT measurement, the sample holder containing each diluted solution (A*−E*, Table 1) was immersed in liquid nitrogen, yielding a homogeneous frozen glass, preventing diffraction from crystals during the data collection. The final $C_{Pb^{2+}}$ was 10 mM for the samples used for ESI-MS, Pb L_{III}-edge EXAFS at RT and LT [33% (v/v) glycerol], ^{207}Pb NMR [10% (v/v) D_2O], ^{1}H NMR (100% D_2O), and UV−vis measurements.

Mass Spectroscopy (MS). MS spectra were collected in negative- and positive-ion modes by direct infusion of the Pb^{2+}-GSH solutions into the ESI source of a Bruker Esquire 3000 mass spectrometer using a continuous injection flow rate of 0.06 mL min^{-1}. The drying gas temperature was 300 °C at 4 L min^{-1} flow rate. The capillary voltage was set at 3.2 kV, for a target mass of m/z 1192; the skimmer voltage was −47.5 V.

NMR Spectroscopy. ^{207}Pb and ^{1}H NMR spectra were collected at 300 K and resonance frequencies of 62.95 and 300.14 MHz, respectively, using a Bruker AMX 300 spectrometer equipped with a 10 mm broad-band probe.

The ^{207}Pb chemical shift was externally calibrated relative to 1.0 M $Pb(NO_3)_2$ in D_2O solution, resonating at −2961.2 ppm relative to $Pb(CH_3)_4$.[57] The ^{207}Pb NMR data were acquired using a 90° pulse, a sweep width of 62.8 kHz, and 64K data points with a 1 s recycle delay between scans. Approximately 10000−40000 scans were coadded. Spectra were processed using exponential line broadening between 25 and 200 Hz (10% of the line width at half-maximum, $\Delta\nu_{1/2}$).

The ^{1}H NMR spectra were collected using a 30° pulse, a sweep width of 3.7 kHz, 16K data points, and a 0.5 s recycle delay between scans. A total of 16 scans were coadded; spectra were referenced internally using the residual HOD/H_2O peak at 4.80 ppm.

Electronic Spectroscopy. UV−vis absorption spectra were measured at RT using a Cary 300 UV−vis double-beam spectrophotometer. Samples were loaded into 1 mm quartz cells; distilled water was used as the blank.

Raman and IR Spectroscopy. The Raman spectrum for the $[Pb(GS)]ClO_4$ solid was measured using a Bruker RAM(II) FT-Raman spectrometer equipped with a liquid-dinitrogen-cooled germanium detector by means of the 1064 nm line excitation of a YAG laser at 100 mW and 4 cm^{-1} resolution. The mid-IR spectrum was obtained from a KBr pellet over the range 400−4000 cm^{-1} with 2 cm^{-1} resolution, using a Nicolet Nexus 470 FT-IR spectrometer.

XAS Data Collection. Pb L_{III}-edge XAS spectra for the Pb^{2+}-GSH solutions A−E were collected under dedicated conditions at Beamline 7-3 at the Stanford Synchrotron Radiation Lightsource (SSRL) (3 GeV, 85−100 mA) and at Beamline 12-C at the Photon Factory of High Energy Accelerator Research Organization, Tsukuba, Japan (2.5 GeV, 250−300 mA). The ion chambers I_0 and I_1 (before and after the sample position, respectively) were filled with dinitrogen gas; the ion chamber I_2 (after the calibration foil) was filled with argon gas. The energy of the X-rays was calibrated by assigning the first inflection point of a Pb foil to 13035 eV. Higher-order harmonics were rejected by a rhodium-coated mirror positioned after the Si(220) double-crystal monochromator at SSRL or by detuning of the Si(111) double-crystal monochromator to 50% of the maximum I_0 intensity at the end of the Pb L_{III}-edge scan region (13807 eV) at the Photon Factory.

Solutions A−E were kept in a 5 mm Teflon spacer with 5 μm polypropylene windows for RT EXAFS measurements. The frozen glassy samples (A*−E*) were held in a 2 mm titanium cell with Kapton windows; the sample temperature was maintained at ∼25 K by means of a liquid-helium cryostat. EXAFS spectra were measured by monitoring the Pb L_α fluorescence radiation from the samples using a 19- (Photon Factory) or 30-element (SSRL) germanium detector. Between 8 and 14 scans were collected for each sample, and all scans and detector channels were compared to ensure that no radiation damage had occurred during the XAS measurements. EXAFS data for the solid D-penicillaminatolead(II) compound, PbPen, mixed with boron nitride were collected in transmission mode at RT at SSRL Beamline 9-3, measuring 26 scans to improve the noise level.

XAS Data Analysis. The fluorescence intensity was compared for each channel in all scans to ensure compatibility prior to averaging using the *EXAFSPAK* suite of programs,[58] or for the Photon Factory data the Rigaku *REX2000 2.5.6* program.[59] The EXAFS oscillations were extracted by means of the *WinXAS 3.1* program,[60] using a first-order polynomial over the preedge region, followed by normalization of the edge step. The energy scale was converted into k space, where $k = [(8\pi^2 m_e/h^2)(E - E_0)]^{1/2}$, using a threshold energy of E_0 = 13033.7−13034.8 eV; for PbPen solid, E_0 = 13035.2 eV.

To extract structural parameters, the EXAFS oscillation, $\chi(k)$, was modeled according to the equation

$$\chi(k) = \sum_i \frac{N_i S_0^2(k)}{kR_i^2} |f_{eff}(k)|_i \exp(-2k^2\sigma_i^2) \exp[-2R_i/\Lambda(k)] \sin[2kR_i + \phi_{ij}(k)] \quad (1)$$

where N_i is the number of scatterers at the distance R_i from the absorber in the ith shell, the Debye−Waller (or disorder) parameter σ_i^2 is the mean-square variation in R_i, k is the scattering variable, $|f_{eff}(k)|_i$ is the effective amplitude function, $\phi_{ij}(k)$ is the total phase shift of the absorber−scatterer pair, and $\lambda(k)$ is the photoelectron mean-free path. The amplitude reduction factor $S_0^2(k)$ is directly correlated to the coordination number N_i.

The effective amplitude function $|f_{eff}(k)|_i$, the total phase shift $\phi_{ij}(k)$, and the photoelectron mean-free path $\lambda(k)$ of the $\chi(k)$ model function were obtained ab initio for the relevant atom-pair interactions by means of the *FEFF 7.0* program.[61,62] The crystal structure of the polymeric D-penicillaminatolead(II) complex PbPen,[63,64] which has both short (2.714 Å) and long (3.091 and 3.464 Å) Pb−S bonds, Pb−(O/N) bonds (2.444, 2.451, and 2.720 Å), as well as thiolate-bridged Pb···Pb interactions (4.363 and 4.663 Å), was used in the *ATOMS* program. Least-squares curve fittings of the $\chi(k)$ model function to the k^3-weighted experimental EXAFS data for solutions A−E and samples A*−E* were performed to refine the structural parameters R and σ^2 and, in some cases, also the coordination number N for each type of

dx.doi.org/10.1021/ic300496t | Inorg. Chem. 2012, 51, 6285−6298

interaction. The amplitude reduction factor (S_0^2) was fixed to 0.9, as obtained from the EXAFS data analysis of the penicillaminatolead(II) complex PbPen, while ΔE_0 (a common value for all paths in a model) was allowed to float.

RESULTS

Solid [Pb(AH$_2$)]ClO$_4$. A white 1:1 Pb^{2+}-GSH precipitate formed from the reaction of GSH with $Pb(ClO_4)_2 \cdot 3H_2O$ in the mole ratio 2:1, an outcome similar to that of the 1:1 D-penicillaminatolead(II) compound that crystallizes as a 1:1 PbPen complex, even in 10-fold excess of the ligand.[63] Vibrational spectra (Figure S-1 in the Supporting Information and Table 2) measured for this precipitate show a ν(Cl−O) stretch at 930 cm^{-1} (Raman), as well as $\delta(ClO_4^-)$ vibrations at 624 cm^{-1} and 622 cm^{-1}, verifying that ClO_4^- was incorporated into the compound with the empirical formula [Pb(AH$_2$)]ClO$_4$. The ν(S−H) stretch of GSH at 2525 cm^{-1}, giving rise to a strong band in the Raman spectrum and a weaker band in the IR spectrum, is absent for the solid [Pb(AH$_2$)]ClO$_4$ compound, indicating that the cysteinyl thiol group is deprotonated and coordinated to the Pb^{2+} center. The IR spectrum for the solid [Pb(AH$_2$)]ClO$_4$ has a broad shoulder at 1708 cm^{-1} for ν(C═O) indicating that one of the two GSH carboxyl groups is protonated (−COOH).[65] Therefore, the coordinated GSH with only one negative charge (AH_2^-) in the [Pb(AH$_2$)]ClO$_4$ compound that precipitated at pH 2.5 has a cysteinyl thiolate (S^-), a Glu NH_3^+, a carboxylic (COOH), and a carboxylate (COO^-) group at its Gly/Glu ends.

Table 2. Selected Vibrational Bands with Assignments for the [Pb(AH$_2$)]ClO$_4$ Precipitate (See Figure S-1 in the Supporting Information)

Raman (cm^{-1})		IR (cm^{-1})		
GSH	[Pb(AH$_2$)]ClO$_4$	GSH	[Pb(AH$_2$)]ClO$_4$	assignment[66]
2525 s		2525 w		ν(S−H)
1706 m		1711 s	1708 sh	ν(COOH)
1663 m	1642 m	1661 s		ν(C═O)
1630 m		1627 vs	1632 br	ν(C═O)
1597 sh	1576 br	1600 vs		$\nu_{as}(COO^-)$
1537 w		1539 vs	1540 vs	ν(C−N) + ν(N−H)
1397 s	1388 m	1397 s	1387 br	$\nu_s(COO^-)$
	930 s		920 w	ν(Cl−O)
	624 w		622 m	δ(Cl−O)

Different structural models were tested in the least-squares curve-fitting procedure for the EXAFS spectrum of the solid [Pb(AH$_2$)]ClO$_4$ (Table S-1 in the Supporting Information). The EXAFS oscillation was well modeled with two Pb−O, one Pb−S, and one (or two) Pb···Pb interactions at the mean distances 2.28 ± 0.04, 2.64 ± 0.04, and 4.15 ± 0.05 Å, respectively (models 3 and 4 in Table S-1 in the Supporting Information and Figure 1). The relatively large disorder parameter obtained for the Pb−O path, σ^2 = 0.0066 ± 0.002 Å^2, indicates a wide distribution around the mean distance. The short k range restricts the number of independently refined parameters. When considering two Pb−S paths in the first coordination shell (model 5), one short Pb−S and one long Pb−S′ path (model 6), or two additional long Pb−O′ distances as possible bridging ligand atoms, the result was either higher residual or very high Debye−Waller factors for the longer Pb−(S′/O′) paths.

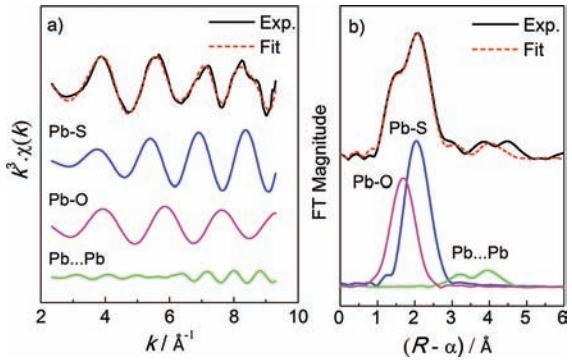

Figure 1. (a) Pb L_{III}-edge EXAFS spectrum for the solid [Pb(AH$_2$)]ClO$_4$ compound with extracted contributions for each scattering path shown below. (b) Corresponding Fourier transforms of EXAFS oscillations (model 3 in Table S-1 in the Supporting Information, including two Pb−O 2.28 ± 0.04 Å, one Pb−S 2.64 ± 0.04 Å, and two Pb···Pb 4.15 ± 0.05 Å).

The comparison between different EXAFS fitting models presented in Table S-1 in the Supporting Information shows that (1) including up to three scattering paths in the fitted model is reasonable, but additional paths with longer distances cause a strong correlation between the parameters and high σ^2 values for the longer paths; (2) even though the coordination number is difficult to determine (see below) for each type of scattering path (models 2−4), there is clearly only one Pb−S path in the first coordination shell of the Pb^{2+} ion, as evidenced by the poor fit for model 5 with the highest residual $\mathcal{R}$; (3) the refined bond distances are quite consistent for all fitting models (except model 5): Pb−O 2.26−2.29 Å, Pb−S 2.63−2.64 Å, and Pb···Pb 4.14−4.15 Å.

To test the accuracy of the bond distances obtained for the solid [Pb(AH$_2$)]ClO$_4$ compound, the Pb L_{III}-edge EXAFS spectrum of the crystalline penicillaminatolead(II) complex (PbPen) was measured at RT. Its crystal structure (Figure S-2 in the Supporting Information) shows two short Pb−(O/N) bonds at ∼2.45 Å and one Pb−S thiolate bond at 2.714 Å. There are also longer interactions in the coordination sphere with two additional Pb−S distances to the thiolate S atom at 3.091 and 3.464 Å, giving rise to double bridges in an infinite-chain structure with Pb···Pb distances of 4.363 Å, and with one bridging Pb−O distance at 2.720 Å between the chains (with Pb···Pb distances of 4.66 Å).[64] Least-squares curve fitting of the k^3-weighted EXAFS oscillation of PbPen over the k range 2.6−9.5 Å^{-1} was performed with models derived from its crystal structure. A satisfactory fit was obtained with two Pb(N/O) and one Pb−S paths at 2.42 ± 0.04 and 2.68 ± 0.04 Å, respectively, which are slightly (∼0.03 Å) shorter than the corresponding distances in the crystal structure. Attempts to fit longer paths, e.g., Pb−(S′/O′), resulted in very high Debye−Waller factors (∼0.02 Å^2). The amplitude reduction factor (S_0^2) was refined to 0.91 and was later fixed to 0.9 in the EXAFS curve-fitting procedure for [Pb(AH$_2$)]ClO$_4$.

Lead(II) Glutathione Solutions. *ESI-MS.* This technique was used for the aqueous solutions A−E with different GSH/Pb^{2+} mole ratios to study the composition of possible Pb^{2+}-GSH complexes. For all five solutions, the ESI-MS spectra showed ions with identical masses, with changes only in the relative intensity of the peaks. The ESI-MS spectrum for solution E with mole ratio GSH/Pb^{2+} = 10 is shown in Figure 2

dx.doi.org/10.1021/ic300496t | Inorg. Chem. 2012, 51, 6285−6298

with assignments of the prominent peaks for the negatively charged complexes in Table 3.

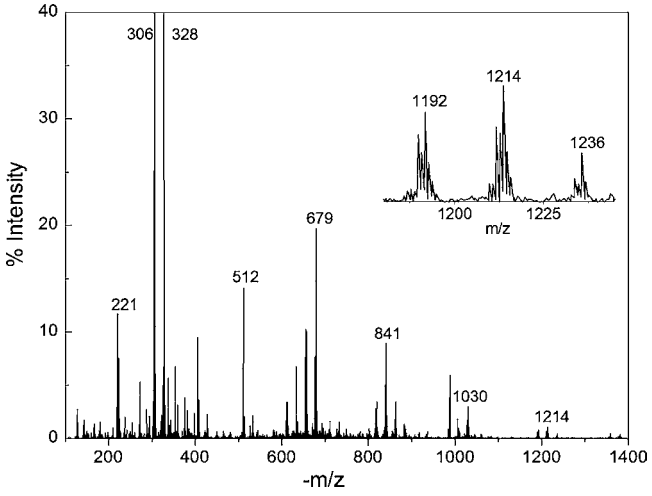

Figure 2. ESI-MS spectrum measured in the negative-ion mode for solution E, mole ratio GSH/Pb^{2+} = 10.0, pH 8.5, $C_{Pb^{2+}}$ = 10 mM. Peaks assigned to $Pb(GSH)_3$ species with ^{208}Pb (Table 3) are shown in the inset.

Table 3. Assignment of Ions Observed in ESI-MS Spectra for the Pb^{2+}-GSH Solutions (pH 8.5, $C_{Pb^{2+}}$ = 10 mM) Measured in the Negative-Ion Mode, as Shown in Figure 2 for Solution E (C_{GSH} = 100 mM)[a]

m/z (amu)	assignment	*m/z* (amu)	assignment
1380.7	$[7Na^+ + (GSH)_4 - 8H^+]^-$	678.9	$[3Na^+ + (GSH)_2 - 4H^+]^-$
1358.7	$[6Na^+ + (GSH)_4 - 7H^+]^-$	656.9	$[2Na^+ + (GSH)_2 - 3H^+]^-$
1235.7	$[5Na^+ + Pb(GSH)_3 - 8H^+]^-$	632.9	$[Na^+ + GSSG - 2H^+]^-$
1213.7	$[4Na^+ + Pb(GSH)_3 - 7H^+]^-$	612.8	$[(GSH)_2 - H^+]^-$
1191.8	$[3Na^+ + Pb(GSH)_3 - 6H^+]^-$	610.9	$[GSSG - H^+]^-$
1029.9	$[5Na^+ + (GSH)_3 - 6H^+]^-$	511.9	$[Pb(GSH) - 3H^+]^-$
862.8	$[2Na^+ + Pb(GSH)_2 - 5H^+]^-$	405.9	$[ClO_4^- + GSH]^-$
840.8	$[Na^+ + Pb(GSH)_2 - 4H^+]^-$	327.9	$[Na^+ + GSH - 2H^+]^-$
818.8	$[Pb(GSH)_2 - 3H^+]^-$	305.9	$[GSH - H^+]^-$
		220.8	$[GSH - Glu]^-$

[a]GSH ($C_{10}H_{17}N_3O_6S$), *m* = 307.3; GSSG ($C_{20}H_{32}N_6O_{12}S_2$), *m* = 612.6

Strong signals at *m/z* 305.9 (assigned 100% intensity in Figure 2) and 327.9 correspond to the monoanions of the free GSH ligand and a Na-GSH complex, respectively. Oxidized glutathione GSSG (*m/z* 632.9 and 610.9) and adduct anions of $(GSH)_n$, where *n* = 2 (*m/z* 612.8, 656.9, and 678.9), 3 (*m/z* 1029.9), or 4 (*m/z* 1358.7 and 1380.7) were observed in the ESI-MS spectra. Higher-order adducts of $(GSH)_n$ (where *n* = 3−5) have also been reported in previous ESI-MS studies of GSH solutions at acidic pH in the positive-ion mode.[44]

Assignments to Pb^{2+}-GSH complexes are facilitated by the characteristic Pb isotopic distribution with 52.4% ^{208}Pb, 22.1% ^{207}Pb, 24.1% ^{206}Pb, and 1.4% of ^{204}Pb present in natural abundance.[67] Negatively charged $Pb(GSH)_3$ complexes were detected for peaks at *m/z* 1235.7, 1213.7, and 1191.8 in ion pairs with the expected number of H^+ or Na^+ ions paired with the ionizable donor atoms on GSH (Table 3). In addition, similar negatively charged Pb(GSH) (*m/z* 511.9) and $Pb(GSH)_2$ (*m/z* 862.8, 840.8, and 818.8) species were characterized, which may have formed by dissociation of the GSH ligands in a $Pb(GSH)_3$ complex.

In the positive-ion mode, the ESI-MS spectra were dominated by GSH and $(GSH)_n$ adducts (Figure S-4 and Table S-2 in the Supporting Information). Peaks attributed to Pb(GSH) and $Pb(GSH)_2$ species had much lower intensity than in the negative-ion mode, and no peaks corresponding to $Pb(GSH)_3$ species could be detected.

^{1}H NMR Spectroscopy. For Pb^{2+}-GSH solutions A−E, only one set of proton resonances is observed for both coordinated and free GSH molecules, indicative of fast exchange on the NMR time scale (Figure 3). The downfield shift of the Cys *β*

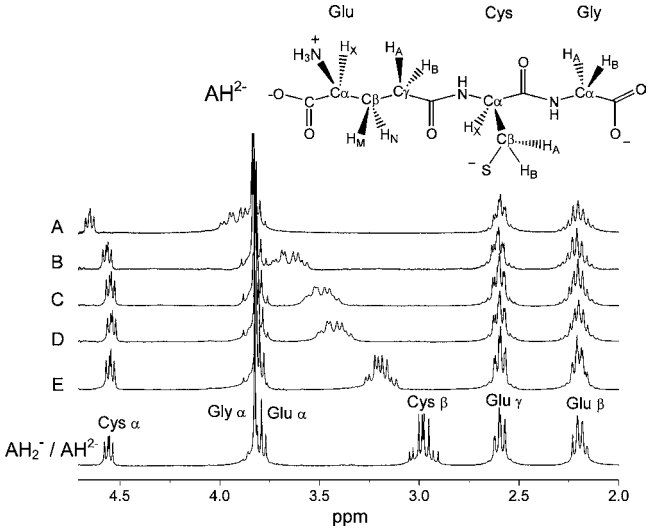

Figure 3. ^{1}H NMR spectra of solutions A−E with GSH/Pb^{2+} mole ratios 2.0 (A), 3.0 (B), 4.0 (C), 5.0 (D), and 10.0 (E) ($C_{Pb^{2+}}$ = 10 mM) in 100% D_2O, compared with free GSH[39] (as AH_2^-/AH^{2-}) at pD 8.9 (measured pH 8.5).[68] The chemical shift is referenced relative to the H_2O/HOD peak at 4.80 ppm; changes in the chemical shifts relative to free GSH are given in Table S-3 in the Supporting Information.

protons for the above solutions and of the Cys *α* proton for solutions A and B indicates that at pH 8.5 the cysteinyl thiolate group is coordinated to the Pb^{2+} center. The Glu *α* proton also shows a small downfield shift in particular for solution A, which implies possible coordination of Glu COO^- or deprotonated amine groups to the Pb^{2+} ion (Table S-3 in the Supporting Information). The Gly COO^- group of GSH is not coordinated because the chemical shift of the Gly *α* protons does not shift downfield relative to the free ligand. Solutions C−E contain increasingly higher excess of GSH (C_{GSH} = 40−100 mM), and the ^{1}H NMR signals begin to resemble that of free GSH.

Electronic Absorption Spectroscopy. In the UV−vis spectra for the Pb^{2+}-GSH solutions A−E (Figure 4), two strong transitions were observed at ∼280 nm and between 317 and 335 nm, which have been assigned to the combination of both S 3p → Pb^{2+} 6p ligand-to-metal charge-transfer (LMCT) and intraatomic Pb^{2+} $6s^2$ → Pb^{2+} 6p transitions.[1,17,18,69] Similar electronic transitions have been observed for three-coordinate PbS_3 complexes to cysteine-rich metalloregulatory pro-

dx.doi.org/10.1021/ic300496t | Inorg. Chem. 2012, 51, 6285−6298

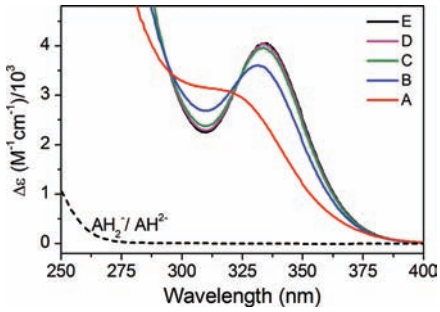

Figure 4. UV−vis spectra of Pb^{2+}-GSH solutions A−E with $C_{Pb^{2+}}$ = 10 mM and mole ratios GSH/Pb^{2+} = 2.0 (A), 3.0 (B), 4.0 (C), 5.0 (D), and 10.0 (E) compared with free GSH as AH_2^-/AH^{2-} at pH 8.5.

teins,[14−16,18,70] as well as structural Zn^{2+} binding domains.[1,17,69,71]

The most blue-shifted absorption spectrum was observed for solution A (GSH/Pb^{2+} = 2.0). The LMCT band had a peak maximum of 317 nm and a noticeably lower molar absorptivity (3100 M^{-1} cm^{-1}) than those for solutions B−E (3611−4054 M^{-1} cm^{-1}; see Figure 4). For solution B with the mole ratio GSH/Pb^{2+} = 3.0, the LMCT transition is slightly blue-shifted to 330 nm relative to that of solutions C−E, with a smaller reduction in the molar absorptivity. Almost identical UV−vis spectra were obtained for solutions C−E (mole ratios GSH/Pb^{2+} = 4.0, 5.0, and 10.0, respectively) with a LMCT transition maximum at 335 nm.

^{207}Pb NMR Spectroscopy. The sensitivity of the NMR resonances to changes in the coordination and bonding environment makes it a useful complement to the structural information from EXAFS spectroscopy. To evaluate the coordination environment around the Pb^{2+} ion in solutions A−E, ^{207}Pb NMR spectroscopy was employed. The ^{207}Pb nucleus has a natural abundance of 22.1%, $I = {}^1/_2$, receptivity of 11.7 relative to ^{13}C, a large chemical shift range (~17000 ppm), giving excellent sensitivity to changes in the metal coordination environment.[57] Generally, ligands with higher polarizability have less shielding effect on the Pb nucleus. Thus, for biologically relevant donor atoms such as S, O, and N, the shielding increases in the order S < N < O.[57] The same trend is observed in the NMR spectra of other heavy-metal $I = {}^1/_2$ nuclei such as ^{199}Hg and $^{111/113}$Cd, with numerous chemical shift values available in the literature for a wide range of different types of Hg^{2+}/Cd^{2+} coordination environments.[72] However, there is still a lack of information, in particular for lead (II) thiolate complexes, to make the ^{207}Pb chemical shift scale reliably useful in a similar way because peptides and proteins containing cysteine are major biological targets for the heavy metal. The ^{207}Pb chemical shifts reported for Pb^{2+} sulfur-coordinated complexes in Figure S-5 in the Supporting Information are shown in Table 4.

No ^{207}Pb NMR resonance could be detected for solution A, not even when a solution with $C_{Pb^{2+}}$ = 90 mM and the same mole ratio GSH/Pb^{2+} = 2.0 was tested. Also, for solution B ($C_{Pb^{2+}}$ = 10 mM and GSH/Pb^{2+} = 3.0), no ^{207}Pb NMR resonance was detected, but a more concentrated solution I ($C_{Pb^{2+}}$ = 90 mM and GSH/Pb^{2+} = 3.0) produced a very broad ^{207}Pb NMR signal centered at 2716 ppm with a large width at half-height, $\Delta\nu_{1/2}$ ~ 2000 Hz. The ^{207}Pb NMR spectra for the Pb^{2+}-GSH solutions C−E ($C_{Pb^{2+}}$ =10 mM and C_{GSH} = 40−100 mM) show a single resonance in a relatively narrow range, 2775−2793 ppm (Figure 5).

Table 4. ^{207}Pb NMR Chemical Shifts Reported for Lead(II) Coordination Sites Containing Sulfur Ligands[a]

coordination environment	chemical shift (δ, ppm)	ref
PbS_3	2818−2868	74, 75
PbS_3 (peptides)	2577−2853	53
PbS_2NS' [b,c]	2873	76
PbS_2N [c]	2852	76
PbS_2N_2 [c]	2733	76
$PbSN_2$	2357	77
PbS_2O_2	1506−1555	78
PbS_3O_3	1422−1463	79

[a]Relative to $Pb(CH_3)_4$ (δ = 0), by setting the ^{207}Pb chemical shift for 0.1 M $Pb(NO_3)_2$ in D_2O at −2961.2 ppm. For information about the types of ligands, see the text and Figure S-5 in the Supporting Information. [b]S′ is a bridging thiolate. [c]Solid-state ^{207}Pb NMR.

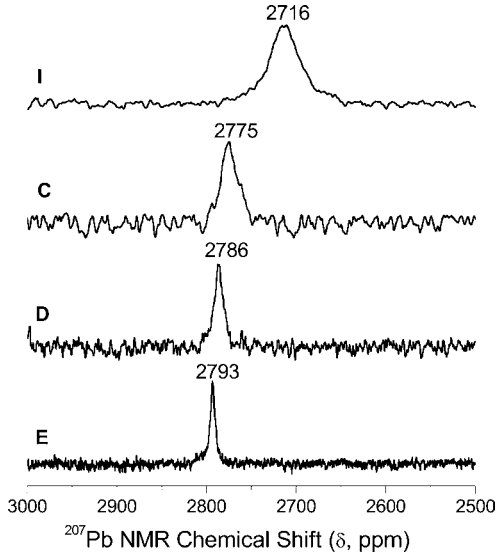

Figure 5. ^{207}Pb NMR spectra of aqueous solutions C−E (GSH/Pb^{2+} mole ratios 4.0, 5.0, and 10.0, respectively), containing 10% D_2O, $C_{Pb^{2+}}$ = 10 mM at pH 8.5 and 300 K. A broad signal was obtained for the concentrated solution I with $C_{Pb^{2+}}$ = 90 mM and GSH/Pb^{2+} = 3.0 at pH 8.5.

For lower GSH/Pb^{2+} mole ratios, the ^{207}Pb NMR chemical shifts became slightly more shielded and increasingly broad. Because lead (II) thiolate bonds are labile, the significant broadening of the ^{207}Pb resonance for concentrated solution I ($C_{Pb^{2+}}$ = 90 mM; GSH/Pb^{2+} = 3.0) is likely due to the intermediate exchange rate between different Pb^{2+}-GSH species at RT. Exchange-broadened line widths have also been previously observed in ^{207}Pb NMR investigations of the Pb^{2+}-substituted Ca^{2+}-binding proteins parvalbumin and calmodulin.[73] A broadening was also observed for the signal at 2777 ppm at pH 7.5 for a solution containing $C_{Pb^{2+}}$ = 5 mM and GSH/Pb^{2+} = 3.0.[55]

Pb L_{III}-Edge X-ray Absorption Near-Edge at RT. The Pb L_{III}-edge XAS near-edge structure (XANES) regions are very similar for solutions B−E (mole ratio GSH/Pb^{2+} ≥ 3.0), showing a broad feature at ~13055 eV characteristic of lead (II) thiolate complexes (Figure 6).[17] For solution A with a lower mole ratio (GSH/Pb^{2+} = 2.0), the slight shift to 13052 eV indicates a slightly different coordination environment. The k^3-weighted EXAFS spectra and corresponding Fourier transforms (FTs) for solutions A−E are shown in Figure 7. Structural

dx.doi.org/10.1021/ic300496t | Inorg. Chem. 2012, 51, 6285−6298

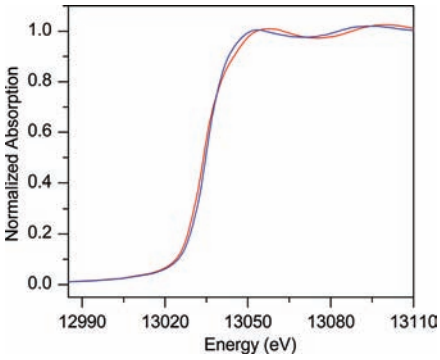

Figure 6. Pb L_{III}-edge XANES spectra at RT for Pb^{2+}-GSH solutions A (blue; E_0 = 13034.8 eV) and E (red; E_0 = 13033.9 eV) with $C_{Pb^{2+}}$ = 10 mM, pH 8.5, and GSH/Pb^{2+} mole ratios 2.0 and 10.0, respectively (E_0 is the inflection point of the rising edge).

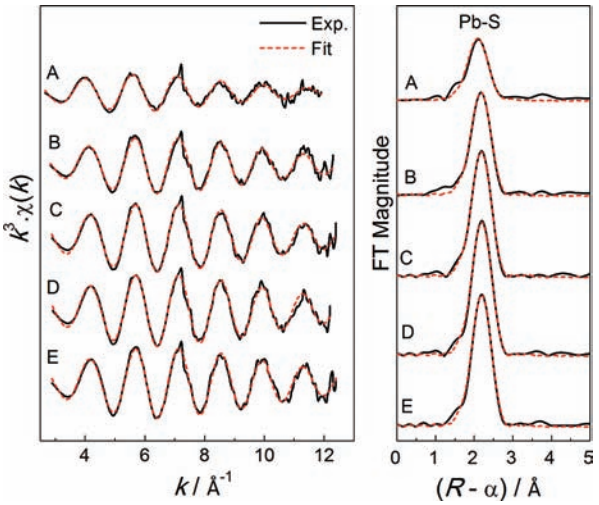

Figure 7. (Left) Pb L_{III}-edge EXAFS spectra for Pb^{2+}-GSH solutions at RT with $C_{Pb^{2+}}$ = 10 mM, pH 8.5 for the mole ratios GSH/Pb^{2+} 2.0 (A), 3.0 (B), 4.0 (C), 5.0 (D), and 10.0 (E). (Right) Corresponding FTs of EXAFS data; see Table 5.

parameters for the Pb^{2+}-GSH complexes formed at RT were obtained by least-squares curve fitting of models to the Pb L_{III}-edge EXAFS oscillations and are presented in Tables 5 and S-4 in the Supporting Information.

The FT magnitude of the EXAFS oscillation for solution A (GSH/Pb^{2+} = 2.0) is noticeably smaller than that of solution E (GSH/Pb^{2+} = 10.0), indicating a lower Pb−S coordination number for A (Figure 7). As the GSH/Pb^{2+} mole ratio increased from 2.0 (solution A) to 3.0 (solution B), the EXAFS amplitude gained intensity, and the disorder parameter for the Pb−S path decreased to σ^2 = 0.005−0.007 Å^2. The very similar EXAFS spectra of solutions B−E were well modeled by three Pb−S bonds at a mean distance of 2.65 ± 0.04 Å. The slightly lower Pb−S coordination number for solution B is reflected by the reduced EXAFS amplitude compared with that for solutions C−E.

Pb L_{III}-Edge XAS at LT. EXAFS data are commonly collected at reduced temperatures to obtain better signal-to-noise ratios and to avoid sample photoreduction. Also, earlier observations have shown that, for Pb^{2+} ions surrounded by O-donor atoms, the average Pb−O distances from EXAFS spectra measured at RT are usually shorter than those obtained at 10 K.[80,81] To study the influence of the temperature on the speciation of

Table 5. Structural Parameters Derived from EXAFS Least-Squares Curve Fitting for the Pb^{2+}-GSH Solutions A−E (pH 8.5, $C_{Pb^{2+}}$ = 10 mM) at RT (See Figure 7)[a−c]

	Pb−S			Pb−(N/O)		
solution (GSH/Pb^{2+} mole ratio)	N	R (Å)	σ^2 (Å^2)	N	R (Å)	σ^2 (Å^2)
A (2.0)	2 f	2.65	0.0156	2 f	2.51	0.0056
B (3.0)	2.9 [d]	2.65	0.0070			
	2 f [e]	2.66	0.0057	2 f	2.49	0.0123
C (4.0)	3.3	2.65	0.0068			
D (5.0)	3.4	2.65	0.0064			
E (10.0)	3.3	2.65	0.0064			

[a]Fitting range: 2.9−12.4 Å^{-1}; S_0^2 = 0.9 f, f = fixed. [b]Refined N is accurate within ±20%. Estimated error limits: R ± 0.04 Å, σ^2 ± 0.002 Å^2. [c]Alternative EXAFS fitting models are presented in Table S-4 in the Supporting Information. [d]The PbS_3 model is shown in Figure 7. [e]PbS_2N_2 model accounting for nitrogen coordination, as shown in Scheme 3.

Pb^{2+}-GSH complexes and the mean Pb−S bond distances, Pb L_{III}-edge XAS spectra were measured at ∼25 K for a series of frozen glycerol/water (33/67, v/v) glasses A*−E* (Table 1). Least-squares curve fitting of the EXAFS spectra for the Pb^{2+}-GSH glassy solutions at LT are shown in Figures 8 (A*) and 9 (B*−E*), with structural parameters summarized in Table 6 and alternative fitting models in Table S-5 in the Supporting Information.

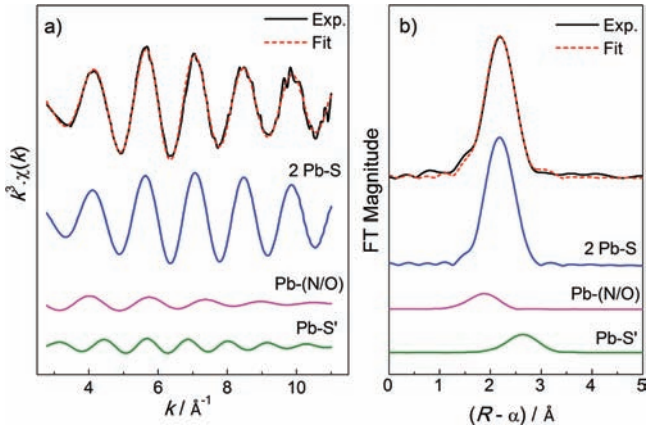

Figure 8. (a) Pb L_{III}-edge EXAFS spectrum for the frozen glass A* at ∼25 K, with separate contributions from the Pb−S, Pb−(N/O), and Pb−S′ scattering paths below; $C_{Pb^{2+}}$ = 10 mM, GSH/Pb^{2+} = 2.0, 33% (v/v) glycerol, and pH 8.5. (b) Corresponding FTs of the EXAFS oscillations (see Table 6).

For the frozen glass A* with GSH/Pb^{2+} = 2.0, the FT magnitude is smaller than that of E* with high excess of GSH, indicating a lower Pb−S coordination number for A*. This is analogous to the smaller FT magnitude for solution A compared to E at RT. For glass B* with mole ratio GSH/Pb^{2+} = 3.0, the FT magnitude is slightly smaller than for the very similar FTs of C*, D* and E* with GSH/Pb^{2+} = 4.0, 5.0, and 10.0, respectively (Figure S-6 in the Supporting Information).

DISCUSSION

Structure of Solid $[Pb(AH_2)]ClO_4$. The vibrational spectra for this solid show that the Pb^{2+} ion is coordinated to GSH via

dx.doi.org/10.1021/ic300496t | Inorg. Chem. 2012, 51, 6285−6298

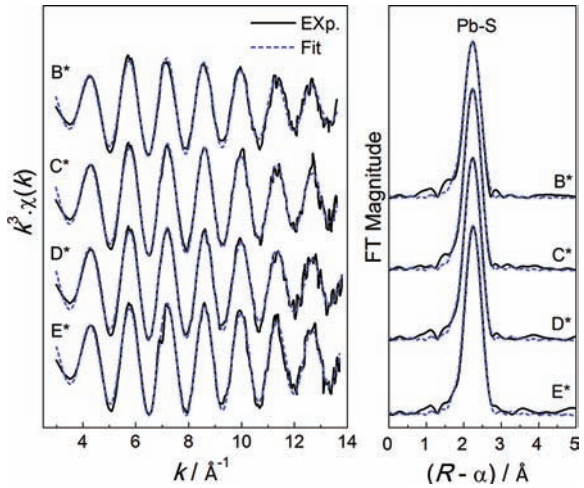

Figure 9. (Left) Pb L_{III}-edge EXAFS spectra for Pb^{2+}-GSH frozen glasses at ~25 K with GSH/Pb^{2+} mole ratios 3.0 (B*), 4.0 (C*), 5.0 (D*), and 10.0 (E*), $C_{Pb^{2+}}$ = 10 mM, 33% (v/v) glycerol, and pH 8.5. (Right) Corresponding FTs of the EXAFS (see Table 6 for the structural parameters).

Table 6. Structural Parameters Derived from EXAFS Least-Squares Curve-Fitting for the Pb^{2+}-GSH Frozen Glasses (A*–E*) at LT (see Figures 8 and 9)[a–c]

	Pb–S			Pb–(N/O)		
solution (GSH/Pb^{2+} mole ratio)	N	R (Å)	σ^2 (Å^2)	N	R (Å)	σ^2 (Å^2)
A* (2.0)	2 f	2.67	0.0052	1 f	2.40	0.0135
	1 f	3.18	0.0126			
B* (3.0)	3.4	2.65	0.0048			
C* (4.0)	3.6	2.65	0.0044			
D* (5.0)	3.8	2.65	0.0047			
E* (10.0)	3.5	2.65	0.0038			

[a]Fitting range: A* (2.8–11.0 Å^{-1}), B*–E* (3.0–13.8 Å^{-1}); f = fixed, S_0^2 = 0.9 f. [b]Refined N accurate within ±20%. Estimated error limits: R ± 0.04 Å; σ^2 ± 0.001 Å^2. [c]Alternative EXAFS fitting models are presented in Table S-5 in the Supporting Information.

its thiol and one of its carboxyl groups. For GSH, the strong $\nu_{as}(COO^-)$ IR band at 1600 cm^{-1} has broadened and shifted to ~1632 cm^{-1} (IR) for $[Pb(AH_2)]ClO_4$. The $\nu_s(COO^-)$ band observed at 1397 cm^{-1} in the IR spectrum for solid GSH has shifted to 1387 cm^{-1} (IR) for $[Pb(AH_2)]ClO_4$. These shifts in the COO^- vibrations, with a rather large separation, $\Delta_{IR} = \nu_{as}(COO^-) - \nu_s(COO^-) = 1632 - 1387 = 245$ cm^{-1}, indicate a monodentate complex formation of the coordinated carboxylate group with the Pb^{2+} ion.[48,65]

On the basis of the Pb L_{III}-edge EXAFS data analysis, the first coordination shell in the solid $[Pb(AH_2)]ClO_4$ compound contains one Pb–S bond at 2.64 ± 0.04 Å and two Pb–O bonds at a mean distance of 2.28 ± 0.04 Å (model 3; Table S-1 in the Supporting Information), forming a distorted $PbSO_2$ trigonal pyramid with a void over the Pb atom in the apex position created by a stereochemically active electron pair. Recently, it was suggested based on energy minimization calculations that monomeric complexes are formed in $[Pb(AH_2)X]\cdot H_2O$ (X = Cl^-, NO_3^-, CH_3COO^-, and NCS^-) compounds, where the Pb^{2+} ion coordinates the X ligand together with one S and two O atoms from the surrounding Cys thiolate, Gly amide C=O and carboxylic C=O groups, in tetrahedral coordination geometry. Both the Glu and Gly carboxylic groups were assumed to be protonated (–COOH), and the amine group ($-NH_2$) was assumed to be deprotonated.[42] Under our experimental conditions (precipitate at pH 2.5), the amine group is protonated $-NH_3^+$, while the partly deprotonated Gly/Glu carboxylate ($-COO^-$) group, together with the cysteine thiolate and possibly the weakly coordinating amide C=O groups,[82] can bind to the Pb^{2+} ion (Scheme 2). Weak coordination of a ClO_4^- O atom has been observed in the crystal structure of $[PATH\text{-}Pb][ClO_4]$, a biological model for a three-coordinated Pb^{2+} ion with $PbSN_2$ distorted trigonal-pyramidal geometry and a Pb···O–ClO_3^- distance of 2.868 Å (PATH = 2-methyl-1-[methyl(2-pyridin-2-ylethyl)amino]propane-2-thiolato).[77,83] However, the absence of splitting in the IR bands for the ClO_4^- ion excludes a short Pb–O–ClO_3 distance in $[Pb(AH_2)]ClO_4$.

Short Pb–S distances similar to that obtained for solid $[Pb(AH_2)]ClO_4$, 2.64 ± 0.04 Å, have also been observed in

Scheme 2. Possible Structure for the $[Pb(AH_2)]ClO_4$ Precipitate Formed at pH 2.5[a]

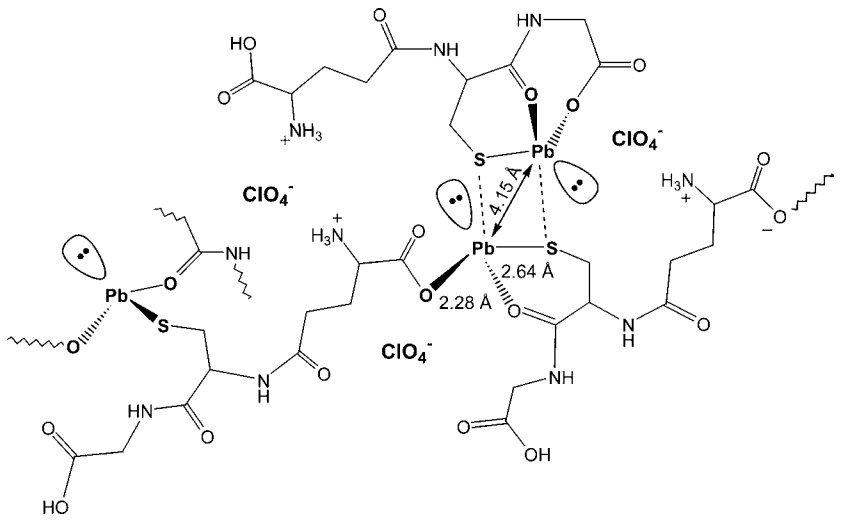

[a]The accuracy of the bond distances is ±0.04–0.05 Å.

dx.doi.org/10.1021/ic300496t | Inorg. Chem. 2012, 51, 6285–6298

Table 7. Survey of Three- and Four-Coordinated Pb^{2+} Complexes Containing S-Donor Ligands (from CSD, version 5.32, Nov 2010;[88] For Details, See Table S-6 in the Supporting Information)

coordination	no. of structures	Pb−S distance range (Å)	average Pb−S distance (Å)	Pb−(O/N) distance range (Å)	average Pb−(O/N) distance (Å)
PbS_4[a]	3	2.65−3.29	2.82		
PbS_3	6	2.55- 2.86	2.70		
PbS_2N	2	2.61−2.79	2.67	2.43−2.61	2.52
PbS_2O	1	2.64	2.64	2.50	2.50
PbS_2N_2	15	2.60−2.92	2.71	2.40−2.85	2.62
PbS_2O_2	6	2.68−2.86	2.75	2.35−2.50	2.40
$PbSN_2$	1	2.59−2.60	2.60	2.49- 2.53	2.51

[a]Lead(II) complexes to dithiocarbamates or S-donor atoms bound to P or Si were not included.

lead (II) complexes with low coordination number. The lead(II) complex with ethanedithiol has two Pb−S bonds at 2.65−2.66 Å.[84] For three-coordinated lead (II) complexes with PbS_3, PbS_2N, and PbS_2O geometries and four-coordinated PbS_2N_2 complexes, the average Pb−S bond distances vary within the range 2.64−2.71 Å; in four-coordinated PbS_2O_2 structures, the average Pb−S distance is slightly longer: 2.75 Å (see Tables 7 and S-6 in the Supporting Information for details). The average Pb−(N/O) distances in three-coordinated lead(II) structures are considerably longer (2.50−.51 Å) than the Pb−O distance 2.28 ± 0.04 Å obtained for $[Pb(AH_2)]ClO_4$. However, similar short Pb−O distances have been obtained in several EXAFS studies for O^{2-}, OH^-, or H_2O ligands; e.g., for Pb^{2+} ions adsorbed on manganese(III, IV) (oxyhydr)oxide minerals (2.28−2.32 Å),[85] on biogenic layers of manganese oxide (2.31−2.32 Å),[86] lead(II) complex formation at a water−Al_2O_3 surface (2.20−2.29 Å),[81] and with lignocellulosic biomaterials (2.35 Å).[87] Also, for crystalline PbO with two short (2.22 Å) and two long Pb−O distances (2.49 Å) in a PbO_4 square-pyramidal geometry, the EXAFS spectrum measured at RT could only show the closest O atoms at Pb−O_{ave} 2.21 Å.[81]

Earlier reports by Manceau et al.[80] and Bargar et al.[81] on the speciation of Pb^{2+} ions surrounded by ligands with O-donor atoms showed that large variations in the Pb−O distances in the first shell, i.e., a distorted coordination environment, result in destructive interference between the Pb−O oscillations that reduces the EXAFS amplitude, which is correlated to the Pb−O coordination number. Self-absorption by Pb^{2+} ions was considered to be a less important factor in reducing the EXAFS amplitude (~3−4%). Modeling the structural disorder with a single scattering path not only increased its σ^2 value but also made determination of the correlated coordination number ambiguous. Also, it was not possible to obtain quantitative information about O atoms at longer distances (beyond the first shell) from the Pb L_{III}-edge EXAFS spectra measured at RT because of the large motion of the atoms. Moreover, both Manceau et al.[80] and Bargar et al.[81] reported that the Pb−O bond distances obtained from RT EXAFS spectra were too short compared to the data collected at 10 K, again a result of a highly asymmetric distribution of the distances. Manceau et al. had obtained the amplitude functions and phase shifts empirically from model compounds,[80] while Bargar et al. used the *FEFF5* program.[81]

The remaining question is whether the $[Pb(AH_2)]ClO_4$ structure is polymeric. PbPen is a polymeric structure with its infinite double chain with Pb···Pb distances at 4.363 Å,[64] while the bis(*N*-methylthioacetohydroxamato)lead(II) structure with PbS_2O_2 coordination geometry and a Pb···Pb separation of 4.05 Å is regarded as monomeric.[89] For $[Pb(AH_2)]ClO_4$, an average Pb···Pb distance of 4.15 ± 0.05 Å was obtained (Table S-1 in the Supporting Information). Because the coordinated Pb−S and Pb−O bond distances are too short to act as bridging ligand atoms, a chain structure is probably formed, where an AH_2^- ligand connects two Pb^{2+} ions by its carboxylate and thiolate groups. A polymeric structure is also possible, similar to that of the lead(II) ethanedithiol complex with short Pb−S bonds (2.65−2.66 Å) and longer interactions (3.05−3.58 Å) in asymmetric bridges to the neighboring Pb^{2+} ions with Pb···Pb distances at 4.20 Å.[84]

Structure of the Pb^{2+}-GSH Complexes in Solution. In the ESI-MS spectra of the lead(II) glutathione solutions A−E, species with not more than three GSH ligands bound to Pb^{2+} could be detected even with high ligand excess (Figure 2 and Table 3). This result differs from that of a recent ESI-MS study in the negative-ion mode, where complex formation of the Pb^{2+} ion with three and four GSH ligands was reported for a solution with $C_{Pb^{2+}}$ = 10 mM and mole ratio GSH/Pb^{2+} = 4.0 at pH 8.[90]

^{1}H NMR spectra of solutions A−E showed a significant downfield shift for Cys β_1 and β_2 protons, indicating that the GSH ligands are coordinated to Pb^{2+} ions via their thiol groups (Figure 3 and Table S-3 in the Supporting Information). In the UV−vis spectra (Figure 4), the $S^- \rightarrow Pb$ LMCT transition appeared as a shoulder at 317 nm for solution A and as a peak with higher molar absorptivity for solutions B (λ_{max} = 330 nm) and C−E (λ_{max} = 335 nm). Similar LMCT bands at ~330 nm have been reported for lead(II) complexes of sulfur-rich proteins and peptides containing three or four cysteine residues.[17,18,69,71,91] Previous UV−vis studies on coordination of the Pb^{2+} ion to metal-binding peptides show a blue shift of the LMCT band from ~330 to ~315 nm, when the number of coordinated cysteine residues to the lead(II) center decreases from three to two, respectively.[71,91] EXAFS investigations on lead (II) complex formation to the metalloregulatory protein CadC revealed a PbS_3 coordination environment with a mean Pb−S distance of 2.66 Å for the wild-type protein and PbS_2O for the C60G mutant (with a similar Pb−S distance of 2.67 Å and a mean Pb−O distance at 2.66 Å). The LMCT bands for these wild-type (PbS_3) and mutant (PbS_2O) proteins were found at 350 and 325 nm, respectively.[15] Comparisons between the LMCT bands observed for the Pb^{2+}-GSH solution and these literature values show that the Pb^{2+} ions are coordinated by two S-donor atoms in A, two or three in solution B, and predominantly three in solutions C−E.

Considering the large chemical shift range (~17000 ppm) in ^{207}Pb NMR spectroscopy, the chemical shifts observed for solutions i (2716 ppm) and C−E and (2775−2793 ppm) are comparable to those reported for lead(II) complexes with PbS_2N_2, PbS_2N, PbS_3, and PbS_2NS' coordination geometries with $\delta(^{207}Pb)$ of 2733, 2852, 2818−2868, and 2873 ppm,

dx.doi.org/10.1021/ic300496t | Inorg. Chem. 2012, 51, 6285−6298

respectively (Table 4).[76] A useful complement to result from the ^{207}Pb NMR technique is provided by structural information from XAS (see below).

GSH/Pb^{2+} Mole Ratio 2.0. The ^{1}H NMR spectrum of solution A showed the largest change in the chemical shift of the Cys β_1 and β_2 protons, with $\Delta\delta$ = 0.95 ppm with respect to free GSH at pH 8.5 (Figure 3 and Table S-3 in the Supporting Information). This is in contrast to a previous ^{1}H NMR study of a D_2O solution containing GSH/Pb^{2+} = 2.0 (at pD 12.9, $C_{Pb^{2+}}$ = 5 mM), where the observed $\Delta\delta$ for the Cys β proton was only 0.23−0.35 ppm.[41] These chemical-shift differences may indicate that speciation of the Pb^{2+}-GSH complexes is different in highly alkaline media, where the amino groups are deprotonated, and hydrolysis of the Pb^{2+} ions is also a competing factor.[92] A closer look at Figure 3 shows that the NMR signal observed for the Glu α proton in free GSH shifts downfield in the spectrum of solution A, which can be attributed to Pb^{2+} coordination to Glu amine or COO$^-$ groups at pH 8.5.

No ^{207}Pb NMR signal could be observed for solution A. Line broadening due to chemical exchange is likely the reason for the absence of a resonance and suggests that mixtures of different Pb^{2+} coordination environments are present for solutions with mole ratios GSH/Pb^{2+} = 2.0.

The EXAFS spectrum of solution A was fitted to different models (Table S-4 in the Supporting Information). When only Pb−S bonds were included in the EXAFS model (I), the coordination number refined to 2.7 at a mean distance of 2.63 ± 0.04 Å. As discussed above, the bond distances between Pb^{2+} and its nearest neighbors obtained from EXAFS oscillation curve fitting at RT are slightly shorter than those obtained from crystallography, as was previously observed, e.g., for the tris(2-mercapto-1-phenylimidazolyl)hydroboratolead complex, with an average Pb−S distance of 2.693 Å from the crystal structure[19] and 2.671 Å from EXAFS spectroscopy.[17] Also, the average Pb−(O/N) and Pb−S bond distances obtained from the EXAFS model fitting to the spectrum of solid PbPen in the current study were slightly shorter (~0.03 Å) than the corresponding crystallographic distances.

The EXAFS spectrum of solution A was also modeled using a combination of Pb−S and Pb−(N/O) scattering pathways, considering the downfield shift of the ^{1}H NMR signal for the Glu α proton in this solution and the maximum absorption of 315 nm in its UV−vis spectrum. Similar fitting residuals were obtained for $PbS_2(N/O)$ or $PbS_2(N/O)_2$ coordination models (II and III in Table S-4 in the Supporting Information), with the mean Pb−S and Pb−(N/O) bond distances at 2.65−2.66 and 2.48−2.51 Å, respectively. The refined Pb−(N/O) distances are considerably longer (~0.2 Å) than that of solid $[Pb(AH_2)]ClO_4$ with $PbSO_2$ coordination geometry and close to those observed for the three-coordinated bis[2,4,6-tris(trifluoromethyl)thiophenolato](tetrahydrofuran)lead(II) (PbS_2O; code KOYFEJ) and bis(2,6-dimethylphenylthiolato)-[4-(dimethylamino)pyridyl]lead(II) (PbS_2N; code XIRCEH) crystal structures and the four-coordinated PbS_2N_2 structures: benzil bis(thiosemicarbazonato)lead(II) (code NOGQOQ) and bis(8-mercaptoquinolinolato)lead(II) (code PBMQNL10). See Table S-6 in the Supporting Information.[76,77,93−95] The large disorder parameter (σ^2) of 0.012−0.016 Å^2 obtained for the Pb−S path represents a wide distribution in the Pb−S bond distances; the formation of mixtures of complexes with $PbS_2(N/O)$ and $PbS_2(N/O)_2$ coordination is likely the reason. Fast ligand exchange in such a mixture probably prevented the observation of a ^{207}Pb NMR resonance for solution A.

The EXAFS spectrum of the frozen glass A* with similar composition ($C_{Pb^{2+}}$ = 10 mM; GSH/Pb^{2+} = 2.0) was fitted with different lead(II) coordination models (Table S-5 in the Supporting Information). For an EXAFS model including only the Pb−S path (model I), the coordination number refined to 2.9 for the mean distance 2.67 ± 0.04 Å, which is longer than that obtained for the corresponding solution A measured at RT using a similar model (2.63 ± 0.04 Å; Table S-4 in the Supporting Information). The best fit was obtained using a $PbS_2(N/O)S'$ coordination model (IV) for which the Pb−S, Pb−(N/O), and the long distance Pb−S′ average path lengths refined to 2.67 ± 0.04, 2.40 ± 0.04, and 3.18 ± 0.05 Å, respectively (Figure 8 and Table 6). Fixing the Pb−O distance at 2.45 Å in the same model fit resulted in very similar refined values and residual because the contribution of this path is diminished by its high disorder parameter (σ^2 = 0.013 Å^2). There is no evidence in the literature for lead(II)−glycerol interactions in such mixtures. However, considering the disordered coordination around Pb^{2+} ions, in general, weak long distance interactions that are difficult to detect cannot be ruled out. For the mercury(II) glutathione system, we have shown that the presence of 33% (v/v) glycerol had no effect on the speciation.[50]

GSH/Pb^{2+} Mole Ratio 3.0. In the ^{1}H NMR spectrum of solution B (GSH/Pb^{2+} = 3.0), only the Cys β protons that are close to the GSH thiol group are significantly deshielded relative to free GSH, with $\Delta\delta$ = 0.65−0.69 ppm (Table S-3 in the Supporting Information). The LMCT band at λ_{max} = 330 nm in the UV−vis spectrum of this solution shows that the Pb^{2+} ions are surrounded by two to three GSH thiol groups (Figure 4).

No ^{207}Pb NMR signal could be observed for this solution, however, by increasing the Pb^{2+} concentration from 10 to 90 mM in solution i (GSH/Pb^{2+} = 3.0); a broad peak with $\delta(^{207}Pb)$ = 2716 ppm appeared that is close to the ^{207}Pb chemical shift of 2733 ppm obtained for the solid $(2,6\text{-}Me_2C_6H_3S)_2Pb(py)_2$ complex with PbS_2N_2 coordination (Table 4).[76] It is also comparable to that of the $[Pb(SPh)_3]^-$ complex with PbS_3 coordination [$\delta(^{207}Pb)$ = 2818 ppm in CD_3OD].[74] Coordination of O-donor atoms to the Pb^{2+} ion are known to cause an upfield shift of the ^{207}Pb NMR resonance (i.e., to lower frequency). For example, in Pb^{2+} complexes to thiohydroxamic ligands with PbS_2O_2 coordination environments, ^{207}Pb NMR resonances have been observed within the range 1493−1555 ppm (in $CDCl_3$).[78]

A recent ^{207}Pb NMR study on 5 mM enriched ^{207}Pb^{2+} aqueous solutions with mole ratios GSH/Pb^{2+} = 3.0 gave a single resonance from 2777 to 2793 to 2797 ppm (converted to the present calibration standard) for pH values from 7.5 to 8.5 to 9.5. This narrow range of chemical shifts was assigned to $Pb(GSH)_3$ as the major species with trigonal-pyramidal PbS_3 coordination geometry.[55] Increasing the mole ratio to GSH/Pb^{2+} = 6.0 (pH 8.0, 25 °C) resulted in a resonance within the same range (2787 ppm).

Least-squares curve fitting of the experimental EXAFS oscillation obtained for solution B using a model with only Pb−S bonds (model I, Table 6) resulted in the mean Pb−S distance 2.65 ± 0.04 Å with a smaller disorder parameter (σ^2 = 0.007 Å^2) than that for A (0.011 Å^2). The refined coordination number of 2.9 for solution B is higher that that of solution A and is reflected in the larger FT peak (Figure 7). Including a

dx.doi.org/10.1021/ic300496t | Inorg. Chem. 2012, 51, 6285−6298

Scheme 3. Proposed Structures for Lead(II) Glutathione Complexes $Pb(GSH)_2$ and $Pb(GSH)_3$ at pH 8.5, with the Latter Dominating in the Solutions Containing $C_{Pb^{2+}}$ = 10 mM and C_{GSH} > 15 mM (for the Distances, See Table 5)

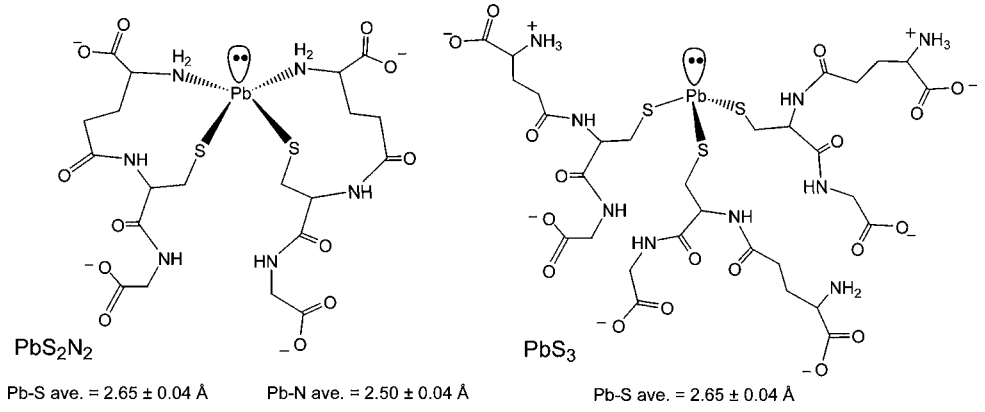

Pb−N path in the models (PbS_2N or PbS_2N_2) resulted in a mean Pb−S distance of 2.65 ± 0.04 Å, while the Pb−N distance varied from 2.45 to 2.49 Å with large disorder parameters (σ^2 = 0.0067 Å^2 for PbS_2N and 0.0123 Å^2 for PbS_2N_2). Note that oxygen and nitrogen cannot be distinguished by EXAFS spectroscopy; however, because of the considerably deshielded ^{207}Pb NMR chemical shifts obtained for the Pb^{2+}-GSH solutions, Pb^{2+}-O coordination (e.g., OH^- or H_2O) does not seem likely at pH 8.5. The coordinated N site of GSH is probably the Glu amine group, as indicated by the small downfield shift of the Glu α proton (Figure 3). It is unlikely that the N atoms of the GSH amide groups coordinate to Pb^{2+} ions: it would require deprotonation and has only been observed for some metal ions at high pH, with the crystal-field stabilization energy being the driving force;[82] this is not the case for Pb^{2+} ions.

The combined results from the UV−vis, ^{207}Pb NMR, and Pb L_{III}-edge EXAFS spectroscopic studies suggest, therefore, that solution B contains a mixture of Pb^{2+}-GSH complexes with PbS_3 and PbS_2N_2 geometries (Scheme 3), where GSH coordinates via its $-NH_2$ and thiol groups to the Pb^{2+} ions, with the mean Pb−S and Pb−N distances 2.66 ± 0.04 and 2.49 ± 0.04 Å, respectively.

The EXAFS spectrum at LT for the glassy solution B* with similar composition was well modeled by a single shell of Pb−S scatterers with the coordination number 3.4. The mean Pb−S distance 2.65 ± 0.04 Å is the same as that obtained for solution B measured at RT, making a PbS_3 coordination environment likely also for the Pb^{2+}-GSH species in B*. Including the Pb−N scattering path in the fitting model either increased the fitting residual or resulted in a high disorder parameter for this path, which is not reasonable at LT (models II and V in Table S-5 in the Supporting Information).

GSH/Pb^{2+} Mole Ratios ≥4.0. The UV−vis spectra of solutions C−E (GSH/Pb^{2+} = 4.0−10.0) display overlapping peaks at 335 nm, showing that three GSH thiol groups are coordinated to the Pb^{2+} ions.[17,71] The ^{207}Pb NMR chemical shifts for solutions C−E in the range 2775−2793 ppm are comparable to the PbS_3 coordinated $[Pb(SPh)_3]^-$ complex with $\delta(^{207}Pb)$ = 2818 ppm in CD_3OD.[74]

The refined Pb−S distance at 2.65 ± 0.04 Å for solutions C−E is comparable with the average Pb−S bonds in crystal structures of three-coordinated PbS_2O, PbS_2N, and PbS_3 and four-coordinated PbS_2N_2 complexes (range 2.64−2.71 Å; see Tables 7 and S-6 in the Supporting Information) and slightly shorter than that of PbS_2O_2 complexes (R_{av} = 2.75 Å). Fitting the EXAFS spectra of these solutions using a PbS_2N_2 model led to slightly longer Pb−S bond distances and reasonable σ^2 values, although with higher residuals than those for the PbS_3 model (Table S-4 in the Supporting Information).

Thus, the combination of UV−vis, ^{207}Pb NMR, and EXAFS spectroscopic results confirms that, in solutions C−E, the $Pb(GSH)_3$ complex is the dominating species with GSH coordinated exclusively via its thiol group with the mean Pb−S distance 2.65 ± 0.04 Å (Scheme 3). Structural studies of Pb^{2+} complex formation to sulfur-rich sites, including Zn^{2+} in peptides and metalloregulatory proteins, also show a preference for a PbS_3 coordination environment, with mean Pb−S distances obtained from EXAFS spectroscopy reported at 2.64 and 2.66 Å, respectively.[15,17] A PbS_4 coordination geometry is unlikely for the Pb^{2+}-GSH complexes because in this case the average Pb−S distance should be ∼2.8 Å (Table S-6 in the Supporting Information), which is more commonly found in polymeric complexes and for Pb^{2+} complexes to dithiocarbamate ligands (not included in Table S-6 in the Supporting Information).

The experimental EXAFS spectra for glasses C*−E* with similar compositions (mole ratios GSH/Pb^{2+} ≥ 4.0) were well modeled by three Pb−S bonds at the mean distance of 2.65 ± 0.04 Å, which is the same mean Pb−S distance observed for the Pb^{2+}-GSH solutions C−E at RT, indicating similar speciation. The smaller Debye−Waller parameter for the Pb−S path, from ∼0.006 Å^2 at RT to ∼0.004 Å^2 at LT, is expected because of the reduced thermal disorder at LT. The addition of a Pb−N path in the fitting model generally did not improve the residual or resulted in a high disorder parameter for this path, which is unexpected at such LT (Table S-5 in the Supporting Information).

■ CONCLUSION

The vibrational spectra of the white precipitate formed in acidic aqueous solutions of GSH and $Pb(ClO_4)_2{\cdot}3H_2O$ were consistent with coordination of one GSH ligand to the Pb^{2+} ion through the cysteinyl thiolate and glutamyl/glycyl carboxylate groups in a $[Pb(AH_2)]ClO_4$ compound containing uncoordinated ClO_4^- groups. Its Pb L_{III}-edge EXAFS spectrum was modeled with two Pb−O bonds at 2.28 ± 0.04 Å and one Pb−S bond at 2.64 ± 0.04 Å and with Pb···Pb interactions at 4.15 ± 0.05 Å. On the basis of these results, a structure with

dx.doi.org/10.1021/ic300496t | Inorg. Chem. 2012, 51, 6285−6298

dimeric species with thiolate S atoms forming an asymmetric bridge between the Pb^{2+} centers is proposed.

In a dilute solution ($C_{Pb^{2+}}$ = 10 mM) with mole ratio GSH/Pb^{2+} = 2.0 (pH 8.5), complexes with $PbS_2(N/O)$ and $PbS_2(N/O)_2$ coordination predominately form, with the mean Pb−S and Pb−(N/O) distances 2.65 ± 0.04 and 2.48−2.51 Å, respectively. The ^{1}H NMR data support that the Cys thiol and Glu amine or COO^- groups are possible ligands to the Pb^{2+} ion. A ^{207}Pb NMR resonance could not be detected for this solution, indicating a mixture of different species and making it difficult to propose whether Glu amine or the more shielding COO^- groups are coordinated.

At the mole ratio GSH/Pb^{2+} = 3.0, a mixture of $Pb(GSH)_2$ and $Pb(GSH)_3$ complexes with PbS_2N_2 and PbS_3 geometries (Scheme 3) is present, giving rise to a broad ^{207}Pb NMR signal at 2716 ppm ($C_{Pb^{2+}}$ = 90 mM), a $S^- \rightarrow Pb^{2+}$ LMCT band at λ_{max} = 330 nm, a slight downfield shift for the Glu α proton, and average Pb−S and Pb−N distances of 2.66 ± 0.04 and 2.49 ± 0.04 Å.

For solutions containing mole ratios GSH/Pb^{2+} ≥ 4.0, three-coordinated PbS_3 complexes predominate, with the mean Pb−S distance 2.65 ± 0.04 Å, a ^{207}Pb NMR chemical shift of 2793 ppm, and a LMCT band at 335 nm. The triglutathionyllead(II) complex with the general formula $[Pb(GSH)_3]^{n-}$ was also detected by ESI-MS and persists even at high excess of the ligand (mole ratio GSH/Pb^{2+} = 10). This complex probably has trigonal-pyramidal PbS_3 geometry (Scheme 3) because the coordination figure mostly is hemidirected with a stereochemically active inert electron pair for coordination numbers below 5. A preference for PbS_3 coordination environments was previously observed for Pb^{2+} bound to large proteins (e.g., cysteine-rich Zn^{2+} structural domains and metalloregulatory proteins).

EXAFS spectra were measured for Pb^{2+}-GSH frozen glasses with $C_{Pb^{2+}}$ = 10 mM and mole ratios GSH/Pb^{2+} = 2.0−10.0 from solutions with pH 8.5 and with 33% (v/v) glycerol. The same Pb−S bond distance of 2.65 ± 0.04 Å was obtained at both RT and LT for solutions containing excess GSH, where $Pb(GSH)_3$ species are dominant, indicating that the highest thiol-coordinated complex formed at LT (PbS_3) is the same as that at RT. This is in contrast to previous results for Hg^{2+}-GSH and Cd^{2+}-GSH alkaline solutions, for which complexes with higher thiolate coordination numbers were found to form at LT.[50,51]

These results for the Pb^{2+} complex formation with GSH have implications for the rational design of chelating agents for the therapeutic treatment of lead poisoning. Currently, the most common compounds used for chelation therapy of Pb^{2+} are *meso*-2,3-dimercaptosuccinic acid, ethylenediaminetetraacetic acid, D-penicillamine, and 2,3-dimercaptopropanol (British Anti-Lewisite).[1,96] One problem associated with these chelating agents is that they are not selective and can also bind essential Fe^{2+}, Ca^{2+}, and Zn^{2+} metal ions, resulting in related toxic effects.[96] A ^{1}H NMR study demonstrated that the tridentate [tris(2-mercapto-1-phenylimidazolyl)hydroborate] ligand chelates to the Pb^{2+} ion with 500-fold affinity over Zn^{2+}, in the S_3 coordination mode.[19] Given that Pb^{2+} prefers to bind a maximum of three GSH ligands through the Cys thiolate group in aqueous solution, our results suggest that a specially tailored chelating agent with three S-donor atoms available for binding could be very efficient in sequestering Pb^{2+} ions.

■ ASSOCIATED CONTENT

Supporting Information

IR and Raman spectra of $[Pb(AH_2)]ClO_4$, crystal structure of D-penicillaminatolead(II), PbPen, used to simulate model EXAFS oscillations, EXAFS fitting of PbPen solid, ESI-MS spectrum of GSH/Pb^{2+} = 10.0 in the positive ion mode, table for the assignment of mass ions in positive-ion mode, table for ^{1}H NMR chemical shift changes for solutions A−E relative to free GSH, table for additional EXAFS fitting results for solutions A−E and A*−E*, structures for Pb^{2+} sulfur-coordinated complexes for which ^{207}Pb NMR chemical shifts are reported, comparison of the EXAFS oscillations of 33% (v/v) glycerol/water frozen glasses with GSH/Pb^{2+} mole ratios of 2.0, 3.0, and 10.0 ($C_{Pb^{2+}}$ = 10 mM, pH 8.5) at LT, and CSD survey of crystal structures with PbS_4, PbS_3, PbS_3N, PbS_2N_2, PbS_2O_2, $PbSN_2$, PbS_2N, and PbS_2O coordination. This material is available free of charge via the Internet at http://pubs.acs.org.

■ AUTHOR INFORMATION

Corresponding Author

*E-mail: faridehj@ucalgary.ca.

Notes

The authors declare no competing financial interest.

■ ACKNOWLEDGMENTS

We are grateful to Qiao Wu and Dorothy Fox at the instrument facility at the Department of Chemistry for their assistance with ESI-MS and NMR measurements. Special thanks go to Professor Serena De Beer for measuring the EXAFS spectrum of the PbPen solid. XAS measurements were carried out at the Photon Factory, Tsukuba, Japan (Proposal No. 2005G226) and SSRL (Proposal No. 2848), a U.S. national user facility operated by Stanford University on behalf of the U.S. Department of Energy, Office of Basic Energy Sciences. The SSRL Structural Molecular Biology Program is supported by the Department of Energy, Office of Biological and Environmental Research, and by the National Institutes of Health, National Center for Research Resources, Biomedical Technology Program. We are grateful to the National Science and Engineering Research Council of Canada, the Canadian Foundation for Innovation, and the Province of Alberta (Department of Innovation and Science) for their financial support.

■ REFERENCES

(1) Claudio, E. S.; Godwin, H. A.; Magyar, J. S. Fundamental coordination chemistry, environmental chemistry and biochemistry of lead(II). In *Progress in Inorganic Chemistry*; Karlin, K. D., Ed.; John Wiley & Sons Inc.: Hoboken, NJ, 2003; Vol. *51*, pp 1−144.
(2) Gidlow, D. A. *Occup. Med.* **2004**, *54*, 76−81.
(3) Needleman, H. *Annu. Rev. Med.* **2004**, *55*, 209−222.
(4) Bressler, J.; Kim, K.-a.; Chakraborti, T.; Goldstein, G. *Neurochem. Res.* **1999**, *24*, 595−600.
(5) Godwin, H. A. *Curr. Opin. Chem. Biol.* **2001**, *5*, 223−227.
(6) Warren, M. J.; Cooper, J. B.; Wood, S. P.; Shoolingin-Jordan, P. M. *Trends Biochem. Sci.* **1998**, *23*, 217−221.
(7) Simons, T. J. B. *Eur. J. Biochem.* **1995**, *234*, 178−183.
(8) Kwong, W. T.; Friello, P.; Semba, R. D. *Sci. Total Environ.* **2004**, *330*, 21−37.
(9) Erskine, P. T.; Duke, E. M. H.; Tickle, I. J.; Senior, N. M.; Warren, M. J.; Cooper, J. B. *Acta Crystallogr., Sect. D* **2000**, *56*, 421−430.

(10) Erskine, P. T.; Newbold, R.; Brindley, A. A.; Wood, S. P.; Shoolingin-Jordan, P. M.; Warren, M. J.; Cooper, J. B. *J. Mol. Biol.* **2001**, *312*, 133−141.
(11) Erskine, P. T.; Senior, N.; Awan, S.; Lambert, R.; Lewis, G.; Tickle, I. J.; Sarwar, M.; Spencer, P.; Thomas, P.; Warren, M. J.; Shoolingin-Jordan, P. M.; Wood, S. P.; Cooper, J. B. *Nat. Struct. Biol.* **1997**, *4*, 1025−1031.
(12) Jaffe, E. K.; Martins, J.; Li, J.; Kervinen, J.; Dunbrack, R. L. *J. Biol. Chem.* **2001**, *276*, 1531−1537.
(13) Apuy, J. L.; Busenlehner, L. S.; Russell, D. H.; Giedroc, D. P. *Biochemistry* **2004**, *43*, 3824−3834.
(14) Busenlehner, L. S.; Giedroc, D. P. *J. Inorg. Biochem.* **2006**, *100*, 1024−1034.
(15) Busenlehner, L. S.; Weng, T.-C.; Penner-Hahn, J. E.; Giedroc, D. P. *J. Mol. Biol.* **2002**, *319*, 685−701.
(16) Liu, T.; Golden, J. W.; Giedroc, D. P. *Biochemistry* **2005**, *44*, 8673−8683.
(17) Magyar, J. S.; Weng, T.-C.; Stern, C. M.; Dye, D. F.; Rous, B. W.; Payne, J. C.; Bridgewater, B. M.; Mijovilovich, A.; Parkin, G.; Zaleski, J. M.; Penner-Hahn, J. E.; Godwin, H. A. *J. Am. Chem. Soc.* **2005**, *127*, 9495−9505.
(18) Wang, Y.; Hemmingsen, L.; Giedroc, D. P. *Biochemistry* **2005**, *44*, 8976−8988.
(19) Bridgewater, B. M.; Parkin, G. *J. Am. Chem. Soc.* **2000**, *122*, 7140−7141.
(20) Shimoni-Livny, L.; Glusker, J. P.; Bock, C. W. *Inorg. Chem.* **1998**, *37*, 1853−1867.
(21) Persson, I.; Lyczko, K.; Lundberg, D.; Eriksson, L.; Płaczek, A. *Inorg. Chem.* **2011**, *50*, 1058−1072.
(22) Walsh, A.; Watson, G. W. *J. Solid State Chem.* **2005**, *178*, 1422−1428.
(23) Mudring, A.-V.; Rieger, F. *Inorg. Chem.* **2005**, *44*, 6240−6243.
(24) Mudring, A.-V. *Eur. J. Inorg. Chem.* **2007**, *2007*, 882−890.
(25) Meister, A. *J. Biol. Chem.* **1988**, *263*, 17205−17208.
(26) Meister, A.; Anderson, M. E. *Annu. Rev. Biochem.* **1983**, *52*, 711−760.
(27) Bae, W.; Mehra, R. K. *J. Inorg. Biochem.* **1997**, *68*, 201−210.
(28) Mehra, R. K.; Kodati, V. R.; Abdullah, R. *Biochem. Biophys. Res. Commun.* **1995**, *215*, 730−736.
(29) Mehra, R. K.; Mulchandani, P. *Biochem. J.* **1995**, *307*, 697−705.
(30) Meister, A.; Tate, S. S. *Annu. Rev. Biochem.* **1976**, *45*, 559−604.
(31) Rauser, W. E. The role of glutathione in plant reaction and adaptation to excess metals. In *Significance of Glutathione in Plant Adaptation to the Environment*; Grill, D., Tausz, M., De Kok, L. J., Eds.; Kluwer Academic Publishers: Dordrecht, The Netherlands, 2001; pp 123−154.
(32) Singhal, R. K.; Anderson, M. E.; Meister, A. *FASEB J.* **1987**, *1*, 220−223.
(33) Zenk, M. H. *Gene* **1996**, *179*, 21−30.
(34) Hunaiti, A. A.; Soud, M. *Sci. Total Environ.* **2000**, *248*, 45−50.
(35) Hunaiti, A.; Soud, M.; Khalil, A. *Sci. Total Environ.* **1995**, *170*, 95−100.
(36) Onunkwor, B.; Dosumu, O.; Odukoya, O. O.; Arowolo, T.; Ademuyiwa, O. *Environ. Toxicol. Pharmacol.* **2004**, *17*, 169−176.
(37) Chai, F.; Wang, C.; Wang, T.; Li, L.; Su, Z. *ACS Appl. Mater. Interfaces* **2010**, *2*, 1466−1470.
(38) Huckerby, T. N.; Tudor, A. J.; Dawber, J. G. *J. Chem. Soc., Perkin Trans. 2* **1985**, 759−763.
(39) Rabenstein, D. L. Metal complexes of glutathione and their biological significance. In *Glutathione: Chemical, Biochemical, and Medical Aspects*; Part, A., Dolphin, D.; Poulson, R.; Avramovic, O., Eds.; John Wiley & Sons: New York, 1989; Vol. *3*, pp 147−186.
(40) Fuhr, B. J.; Rabenstein, D. L. *J. Am. Chem. Soc.* **1973**, *95*, 6944−6950.
(41) Kane-Maguire, L. A. P.; Riley, P. J. *J. Coord. Chem.* **1993**, *28*, 105−120.
(42) Singh, B.; Sharma, R.; Garg, B. *J. Therm. Anal. Calorim.* **2006**, *84*, 593−600.
(43) Corrie, A. M.; Walker, M. D.; Williams, D. R. *J. Chem. Soc., Dalton Trans.* **1976**, 1012−1015.
(44) Burford, N.; Eelman, M. D.; Groom, K. *J. Inorg. Biochem.* **2005**, *99*, 1992−1997.
(45) Cruz, B. H.; Díaz-Cruz, J. M.; Díaz-Cruz, M. S.; Ariño, C.; Esteban, M.; Tauler, R. *J. Electroanal. Chem.* **2001**, *516*, 110−118.
(46) Jalilehvand, F.; Leung, B. O.; Izadifard, M.; Damian, E. *Inorg. Chem.* **2006**, *45*, 66−73.
(47) Jalilehvand, F.; Leung, B. O.; Mah, V. *Inorg. Chem.* **2009**, *48*, 5758−5771.
(48) Jalilehvand, F.; Mah, V.; Leung, B. O.; Mink, J.; Bernard, G. M.; Hajba, L. *Inorg. Chem.* **2009**, *48*, 4219−4230.
(49) Leung, B. O.; Jalilehvand, F.; Mah, V. *Dalton Trans.* **2007**, 4666−4674.
(50) Mah, V.; Jalilehvand, F. *J. Biol. Inorg. Chem.* **2008**, *13*, 541−553.
(51) Mah, V.; Jalilehvand, F. *J. Biol. Inorg. Chem.* **2010**, *15*, 441−458.
(52) Mah, V. Heavy metal complex formation with glutathione. Ph.D. Thesis, University of Calgary, Calgary, Alberta, Canada, 2009.
(53) Neupane, K. P.; Pecoraro, V. L. *Angew. Chem., Int. Ed.* **2010**, *49*, 8177−8180.
(54) Zampella, G.; Neupane, K. P.; De Gioia, L.; Pecoraro, V. L. *Chem.—Eur. J.* **2012**, *18*, 2040−2050.
(55) Neupane, K. P.; Pecoraro, V. L. *J. Inorg. Biochem.* **2011**, *105*, 1030−1034.
(56) Levina, A.; Armstrong, R. S.; Lay, P. A. *Coord. Chem. Rev.* **2005**, *249*, 141−160.
(57) Wrackmeyer, B.; Horchler, K.; Webb, G. A. ^{207}Pb-NMR Parameters. In *Annual Report on NMR Spectroscopy*; Webb, G. A., Ed.; Academic Press: San Diego, CA, 1990; Vol. *22*, pp 249−306.
(58) George, G. N.; Geroge, S. J.; Pickering, I. J. *EXAFSPAK*; Stanford Synchrotron Radiation Lightsource (SSRL): Menlo Park, CA, 2001.
(59) Taguchi, T.; Ozawa, T.; Yashiro, H. *Phys. Scr.* **2005**, *T115*, 205−206.
(60) Ressler, T. *J. Synchrotron Radiat.* **1998**, *5*, 118−122.
(61) Ankudinov, A. L.; Rehr, J. J. *Phys. Rev. B* **1997**, *56*, R1712−R1716.
(62) Zabinsky, S. I.; Rehr, J. J.; Ankudinov, A.; Albers, R. C.; Eller, M. J. *Phys. Rev. B* **1995**, *52*, 2995−3009.
(63) Freeman, H. C.; Stevens, G. N.; Taylor, I. F. *J. Chem. Soc., Chem. Commun.* **1974**, 366−367.
(64) Schell, A. C.; Parvez, M.; Jalilehvand, F. *Acta Crystallogr., Sect. E* **2012**, *68*, m489−m490.
(65) Nakamoto, K. *Infrared and Raman Spectra of Inorganic and Coordination Compounds*, 5th ed.; John Wiley & Sons: New York, 1997; Part B.
(66) Qian, W.; Krimm, S. *Biopolymers* **1994**, *34*, 1377−1394.
(67) *CRC Handbook of Chemistry and Physics*, 80th ed.; CRC Press: Boca Raton, FL, 1999.
(68) Glasoe, P. K.; Long, F. A. *J. Phys. Chem.* **1960**, *64*, 188−190.
(69) Ghering, A. B.; Miller Jenkins, L. M.; Schenck, B. L.; Deo, S.; Mayer, R. A.; Pikaart, M. J.; Omichinski, J. G.; Godwin, H. A. *J. Am. Chem. Soc.* **2005**, *127*, 3751−3759.
(70) Busenlehner, L. S.; Cosper, N. J.; Scott, R. A.; Rosen, B. P.; Wong, M. D.; Giedroc, D. P. *Biochemistry* **2001**, *40*, 4426−4436.
(71) Payne, J. C.; ter Horst, M. A.; Godwin, H. A. *J. Am. Chem. Soc.* **1999**, *121*, 6850−6855.
(72) Öz, G.; Pountney, D. L.; Armitage, I. M. *Biochem. Cell Biol.* **1998**, *76*, 223−234.
(73) Aramini, J. M.; Hiraoki, T.; Yazawa, M.; Yuan, T.; Zhang, M.; Vogel, H. J. *J. Biol. Inorg. Chem.* **1996**, *1*, 39−48.
(74) Arsenault, J. J. I.; Dean, P. A. W. *Can. J. Chem.* **1983**, *61*, 1516−1523.
(75) Dean, P. A. W.; Vittal, J. J.; Payne, N. C. *Inorg. Chem.* **1984**, *23*, 4232−4236.
(76) Briand, G. G.; Smith, A. D.; Schatte, G.; Rossini, A. J.; Schurko, R. W. *Inorg. Chem.* **2007**, *46*, 8625−8637.
(77) Andersen, R. J.; diTargiani, R. C.; Hancock, R. D.; Stern, C. L.; Goldberg, D. P.; Godwin, H. A. *Inorg. Chem.* **2006**, *45*, 6574−6576.

(78) Rupprecht, S.; Franklin, S. J.; Raymond, K. N. *Inorg. Chim. Acta* **1995**, *235*, 185−194.
(79) Burnett, T. R.; Dean, P. A. W.; Vittal, J. J. *Can. J. Chem.* **1994**, *72*, 1127−1136.
(80) Manceau, A.; Boisset, M.-C.; Sarret, G.; Hazemann, J.-L.; Mench, M.; Cambier, P.; Prost, R. *Environ. Sci. Technol.* **1996**, *30*, 1540−1552.
(81) Bargar, J. R.; Brown, G. E., Jr.; Parks, G. A. *Geochim. Cosmochim. Acta* **1997**, *61*, 2617−2637.
(82) Sigel, H.; Martin, R. B. *Chem. Rev.* **1982**, *82*, 385−426.
(83) Harrowfield, J. M.; Skelton, B. W.; White, A. H., *J. Chem. Soc., Dalton Trans.* **1993**.
(84) Dean, P. A. W.; Vittal, J. J.; Payne, N. C. *Inorg. Chem.* **1985**, *24*, 3594−3597.
(85) Matocha, C. J.; Elzinga, E. J.; Sparks, D. L. *Environ. Sci. Technol.* **2001**, *35*, 2967−2972.
(86) Villalobos, M.; Bargar, J.; Sposito, G. *Environ. Sci. Technol.* **2005**, *39*, 569−576.
(87) Dupont, L.; Guillon, E.; Bouanda, J.; Dumonceau, J.; Aplincourt, M. *Environ. Sci. Technol.* **2002**, *36*, 5062−5066.
(88) Allen, F. H. *Acta Crystallogr., Sect. B* **2002**, *B58*, 380−388.
(89) Abu-Dari, K.; Hahn, F. E.; Raymond, K. N. *J. Am. Chem. Soc.* **1990**, *112*, 1519−1524.
(90) Połeć-Pawlak, K.; Ruzik, R.; Lipiec, E. *Talanta* **2007**, *72*, 1564−1572.
(91) Rousselot-Pailley, P.; Sénèque, O.; Lebrun, C.; Crouzy, S.; Boturyn, D.; Dumy, P.; Ferrand, M.; Delangle, P. *Inorg. Chem.* **2006**, *45*, 5510−5520.
(92) Perera, W. N.; Hefter, G.; Sipos, P. M. *Inorg. Chem.* **2001**, *40*, 3974−3978.
(93) Labahn, D.; Brooker, S.; Sheldrick, G. M.; Roesky, H. W. *Z. Anorg. Allg. Chem.* **1992**, *610*, 163−168.
(94) López-Torres, E.; Calatayud, D. G.; Pastor, C. J.; Mendiola, M. A. *Polyhedron* **2008**, *27*, 2507−2512.
(95) Agre, V. M.; Shugam, E. A. *Zh. Strukt. Khim.* **1971**, *12*, 102.
(96) Andersen, O. *Chem. Rev.* **1999**, *99*, 2683−2710.